Geosci. Model Dev., 10, 4723–4742, 2017
https://doi.org/10.5194/gmd-10-4723-2017

Geoscientific Model Development
Open Access

^{231}Pa and ^{230}Th in the ocean model of the Community Earth System Model (CESM1.3)

Sifan Gu[1] **and Zhengyu Liu**[2]

[1]Department of Atmospheric and Oceanic Sciences and Center for Climate Research,
University of Wisconsin-Madison, Madison, WI, USA
[2]Atmospheric Science Program, Department of Geography, The Ohio State University, Columbus, OH, USA

Correspondence: Sifan Gu (sgu28@wisc.edu)

Received: 22 March 2017 – Discussion started: 20 April 2017
Revised: 10 November 2017 – Accepted: 15 November 2017 – Published: 22 December 2017

Abstract. The sediment ^{231}Pa / ^{230}Th activity ratio is emerging as an important proxy for deep ocean circulation in the past. In order to allow for a direct model–data comparison and to improve our understanding of the sediment ^{231}Pa / ^{230}Th activity ratio, we implement ^{231}Pa and ^{230}Th in the ocean component of the Community Earth System Model (CESM). In addition to the fully coupled implementation of the scavenging behavior of ^{231}Pa and ^{230}Th with the active marine ecosystem module (particle-coupled: hereafter p-coupled), another form of ^{231}Pa and ^{230}Th have also been implemented with prescribed particle flux fields of the present climate (particle-fixed: hereafter p-fixed). The comparison of the two forms of ^{231}Pa and ^{230}Th helps to isolate the influence of the particle fluxes from that of ocean circulation. Under present-day climate forcing, our model is able to simulate water column ^{231}Pa and ^{230}Th activity and the sediment ^{231}Pa / ^{230}Th activity ratio in good agreement with available observations. In addition, in response to freshwater forcing, the p-coupled and p-fixed sediment ^{231}Pa / ^{230}Th activity ratios behave similarly over large areas of low productivity on long timescales, but can differ substantially in some regions of high productivity and on short timescales, indicating the importance of biological productivity in addition to ocean transport. Therefore, our model provides a potentially powerful tool to help the interpretation of sediment ^{231}Pa / ^{230}Th reconstructions and to improve our understanding of past ocean circulation and climate changes.

1 Introduction

The sediment ^{231}Pa / ^{230}Th activity ratio has been one major proxy for ocean circulation in the past (e.g., Yu et al., 1996; McManus et al., 2004; Gherardi et al., 2009). Quantities of ^{231}Pa (32.5 ka half-life) and ^{230}Th (75.2 ka half-life) are produced at a constant rate approximately uniformly in the ocean by the α decay of ^{235}U and ^{234}U, respectively, with a production activity ratio of 0.093 (Henderson and Anderson, 2003). Water column ^{231}Pa and ^{230}Th are subject to particle scavenging and transport to sediments (Bacon and Anderson, 1982; Nozaki et al., 1987). Different scavenging efficiency results in different ocean residence time: ^{231}Pa has a residence time of approximately 111 years and ^{230}Th has a residence time of approximately 26 years (Yu et al., 1996). The longer residence time of ^{231}Pa than ^{230}Th makes ^{231}Pa more subject to ocean transport, and therefore in the modern ocean about 45 % of ^{231}Pa produced in the North Atlantic is transported to the Southern Ocean (Yu et al., 1996), resulting in a sediment ^{231}Pa / ^{230}Th activity ratio lower than 0.093 in the North Atlantic and a sediment ^{231}Pa / ^{230}Th activity ratio higher than 0.093 in the Southern Ocean.

The application of the above principle to interpret sediment ^{231}Pa / ^{230}Th as the strength of Atlantic meridional overturning circulation (AMOC), however, can be complicated by other factors, leading to uncertainties in using ^{231}Pa / ^{230}Th as a proxy for past circulation (Keigwin and Boyle, 2008; Lippold et al., 2009; Scholten et al., 2008). In addition to the ocean transport, sediment ^{231}Pa / ^{230}Th is also influenced by particle flux and composition (Chase et al., 2002; Geibert and Usbeck, 2004; Scholten et al., 2008;

Published by Copernicus Publications on behalf of the European Geosciences Union.

Siddall et al., 2007; Walter et al., 1997). The region of a higher particle flux tends to have a higher ^{231}Pa / ^{230}Th (Kumar et al., 1993; Yong Lao et al., 1992), which is referred to as the "particle flux effect" (Siddall et al., 2005). Regional high particle flux in the water column will favor the removal of isotopes into the sediment, which leads to more isotopes transported into this region due to the down-gradient diffusive flux and subsequently more removal of isotopes into the sediment. Since ^{231}Pa has a longer residence time, this effect is more prominent on ^{231}Pa than on ^{230}Th and therefore sediment ^{231}Pa / ^{230}Th will be higher in high-productivity regions. Also, opal is able to scavenge ^{231}Pa much more effectively than ^{230}Th, leading to higher ^{231}Pa / ^{230}Th in high-opal-flux regions such as the Southern Ocean (Chase et al., 2002). Moreover, sediment ^{231}Pa / ^{230}Th is suggested to record circulation change only within 1,000 m above the sediment, instead of the whole water column, complicating the interpretation of sediment ^{231}Pa / ^{230}Th reconstructions (Thomas et al., 2006). For example, sediment ^{231}Pa / ^{230}Th approaching 0.093 during Heinrich Stadial event 1 (HS1) from the subtropical North Atlantic is interpreted as the collapse of AMOC (McManus et al., 2004). If sediment ^{231}Pa / ^{230}Th only the records deepest water mass, it is possible that during HS1, AMOC shoals as opposed to fully collapsing, and yet an increase of deep water imported from the Southern Ocean featuring high ^{231}Pa / ^{230}Th can increase the sediment ^{231}Pa / ^{230}Th approaching the production ratio (0.093) (Thomas et al., 2006). Therefore, it is important to incorporate ^{231}Pa and ^{230}Th into climate models for a direct model–data comparison and to promote a thorough understanding of sediment ^{231}Pa / ^{230}Th as well as past ocean circulation.

The presence of ^{231}Pa and ^{230}Th has been simulated in previous modeling studies (Dutay et al., 2009; Luo et al., 2010; Marchal et al., 2000; Rempfer et al., 2017; Siddall et al., 2005). Marchal et al. (2000) simulates ^{231}Pa and ^{230}Th in a zonally averaged circulation model, using the reversible scavenging model of Bacon and Anderson (1982). Going one step further, Siddall et al. (2005) extends Marchal et al. (2000) by including particle dissolution with prescribed particle export production in a 3-D circulation model. Rempfer et al. (2017) further couples ^{231}Pa and ^{230}Th with an active biogeochemical model and includes boundary scavenging and sediment resuspensions to improve model performance in simulating water column ^{231}Pa and ^{230}Th activity. Here we follow previous studies to implement ^{231}Pa and ^{230}Th into the Community Earth System Model (CESM). Our standard ^{231}Pa and ^{230}Th are coupled with an active marine ecosystem model ("p-coupled") and therefore is influenced by both ocean circulation change and particle flux change. To aid understanding of the influence of the particle flux, we have also implemented an auxiliary version of ^{231}Pa and ^{230}Th ("p-fixed") for which the particle fluxes are fixed at prescribed values. Therefore, p-fixed ^{231}Pa / ^{230}Th is only influenced by ocean circulation change. By comparing the p-fixed ^{231}Pa / ^{230}Th with the p-coupled ^{231}Pa / ^{230}Th, we will be able to separate the effect of circulation change from particle flux change. In addition, the p-fixed ^{231}Pa and ^{230}Th can be run without the marine ecosystem module, reducing computational cost by a factor of 3 in the ocean-alone model simulation, making it a computationally efficient tracer for sensitivity studies.

This paper describes the details of ^{231}Pa and ^{230}Th in CESM and serves as a reference for future studies using this tracer module. In Sect. 2, we describe the model and the implementation of ^{231}Pa and ^{230}Th. In Sect. 3, we describe the experimental design. We will finally compare simulated ^{231}Pa and ^{230}Th fields with observations, show model sensitivities to model parameters and also the sediment ^{231}Pa / ^{230}Th ratio response to freshwater forcing in Sect. 4.

2 Model description

2.1 Physical ocean model

We implement ^{231}Pa and ^{230}Th in the ocean model (Parallel Ocean Program version 2, POP2) (Danabasoglu et al., 2012) of CESM (Hurrell et al., 2013). CESM is a state-of-the-art coupled climate model and studies describing model components and analyzing results can be found in a special collection in Journal of Climate (http://journals.ametsoc.org/topic/ccsm4-cesm1). We run the ocean-alone model, which is coupled to data atmosphere, land, ice and river runoff under the normal year forcing of CORE-II data (Large and Yeager, 2008), using the low-resolution version of POP2 with a nominal 3° horizontal resolution and 60 vertical layers.

2.2 Biogeochemical component (BGC)

CESM has incorporated a marine ecosystem module that simulates biological variables (Moore et al., 2013). The marine ecosystem module has been validated against present-day observations extensively (e.g., Doney et al., 2009; Long et al., 2013; Moore et al., 2002, 2004; Moore and Braucher, 2008). The implementation of ^{231}Pa and ^{230}Th requires particle fields: $CaCO_3$, opal and particulate organic carbon (POC). These particle fields can be obtained through the ecosystem driver from the ecosystem module (Jahn et al., 2015). The ecosystem module simulates the particle fluxes in reasonable agreement with the present-day observations. The pattern and magnitude of the annual mean particle fluxes ($CaCO_3$, opal, POC) leaving the euphotic zone at 105 m are similar to those of the satellite observations (Figs. 7.2.5 and 9.2.2 in Sarmiento and Gruber, 2006) (Fig. 1a–c): particle fluxes are higher in the high-productivity regions such as high latitudes and equatorial Pacific; opal flux is high in the Southern Ocean. The remineralization scheme of particles is based on the ballast model of Armstrong et al. (2002). Detailed parameterizations for particle remineralization are documented in Moore et al. (2004) with temperature-dependent remineralization length scales for POC and opal. We do not consider dust because it is suggested to be unimportant for ^{231}Pa and ^{230}Th fractionation (Chase et al., 2002; Siddall et al., 2005).

2.3 ^{231}Pa and ^{230}Th implementation

^{231}Pa and ^{230}Th are produced from the α decay of ^{235}U and ^{234}U uniformly everywhere at constant rate β^i ($\beta^{\mathrm{Pa}} = 2.33 \times 10^{-3}\,\mathrm{dpm\,m^{-3}\,yr^{-1}}$, $\beta^{\mathrm{Th}} = 2.52 \times 10^{-2}\,\mathrm{dpm\,m^{-3}\,yr^{-1}}$). The ^{231}Pa and ^{230}Th are also subjective to radioactive decay with the decay constant of λ^i ($\lambda^{\mathrm{Pa}} = 2.13 \times 10^{-5}\,\mathrm{yr^{-1}}$, $\lambda^{\mathrm{Th}} = 9.22 \times 10^{-6}\,\mathrm{yr^{-1}}$).

Another important process that contributes to ^{231}Pa and ^{230}Th activity is the reversible scavenging by sinking particles (Bacon and Anderson, 1982), which describes the adsorption of isotopes onto sinking particles and desorption after the dissolution of particles. This process transports ^{231}Pa and ^{230}Th downward and leads to a general increase of ^{231}Pa and ^{230}Th activity with depth. The reversible scavenging considers total isotope activity (A_{t}^i) as two categories (Eq. 1): dissolved isotopes (A_{d}^i) and particulate isotopes (A_{p}^i) (superscript i refers to ^{231}Pa and ^{230}Th) and A_{p}^i is the sum of the isotopes associated with different particle types ($A_{j,\mathrm{p}}^i$) (subscript j refers to different particle types: $CaCO_3$, opal and POC):

$$A_{\mathrm{t}}^i = A_{\mathrm{d}}^i + A_{\mathrm{p}}^i = A_{\mathrm{d}}^i + \sum_j A_{j,\mathrm{p}}^i \,. \tag{1}$$

Dissolved and particulate isotopes are assumed to be in equilibrium, which is a reasonable assumption in the open ocean (Bacon and Anderson, 1982; Henderson et al., 1999; Moore and Hunter, 1985). The ratio between the particulate isotope activity and the dissolved isotope activity is set by a partition coefficient, K (Eq. 2):

$$K_j^i = \frac{A_{j,\mathrm{p}}^i}{A_{\mathrm{d}}^i \cdot R_j}\,, \tag{2}$$

where R_j is the ratio of particle concentration (C_j) to the density of seawater ($1024.5\,\mathrm{kg\,m^{-3}}$). Subscript j refers to different particle types ($CaCO_3$, opal and POC). Values of partition coefficient K used in our control simulation follow Chase et al. (2002) and Siddall et al. (2005) (Table 2).

Particulate isotopes (A_{p}^i) will be transported by sinking particles, which is described by $w_{\mathrm{s}} \frac{\partial A_{\mathrm{p}}^i}{\partial z}$ (Eq. 3), where w_{s} is the sinking velocity. We do not differentiate between slowly sinking small particles and rapidly sinking large particles as in Dutay et al. (2009) and consider all particles as slowly sinking small particles with sinking velocity of $w_{\mathrm{s}} = 1000\,\mathrm{m\,yr^{-1}}$ (Arsouze et al., 2009; Dutay et al., 2009; Kriest, 2002), which is similar to Rempfer et al. (2017) and Siddall et al. (2005). Any particulate isotopes (A_{p}^i) at the ocean bottom layer are removed from the ocean as sediment, which is the sink for the isotope budget. A detailed vertical differentiation scheme to calculate this term in the model is provided in the supplementary material. The reversible scavenging scheme applied here is the same as the neodymium implementation in POP2 (Gu et al., 2017).

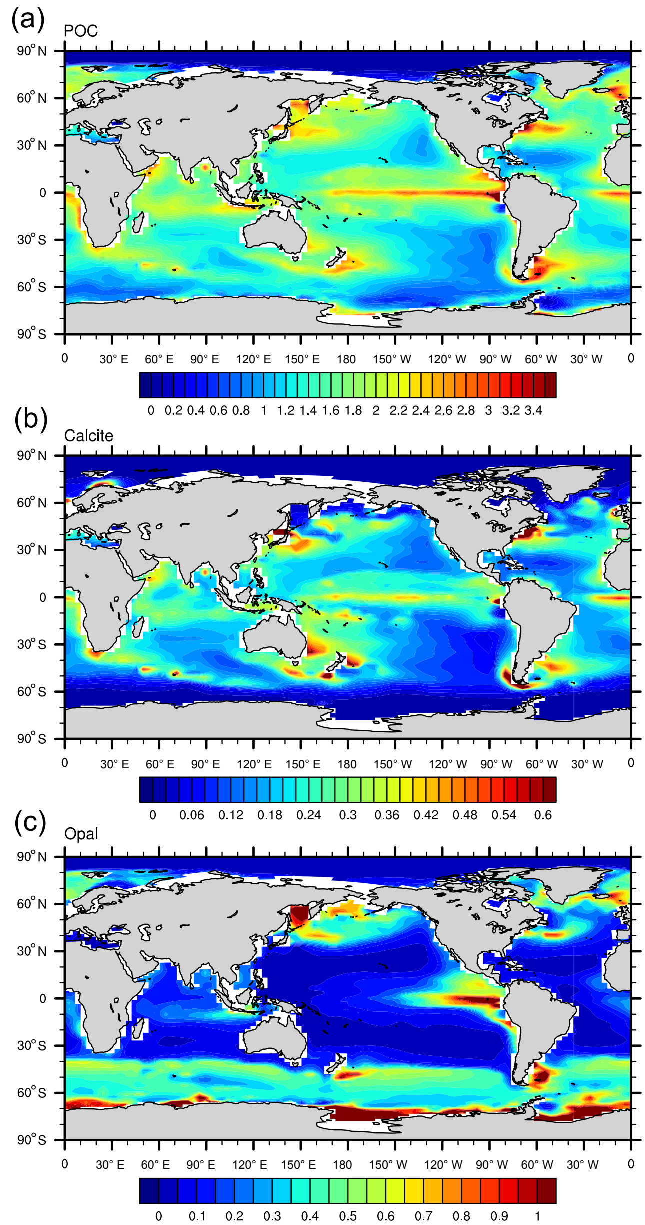

Figure 1. Annual mean particle fluxes in CESM. **(a)** $CaCO_3$ flux at 105 m ($\mathrm{mol\,m^{-2}\,yr^{-1}}$). **(b)** Opal flux at 105 m ($\mathrm{mol\,m^{-2}\,yr^{-1}}$). **(c)** POC flux at 105 m ($\mathrm{mol\,m^{-2}\,yr^{-1}}$).

Therefore, the conservation equation for ^{231}Pa and ^{230}Th activity can be written as

$$\frac{\partial A_{\mathrm{t}}^i}{\partial t} = \beta^i - \lambda^i A_{\mathrm{t}}^i - w_{\mathrm{s}} \frac{\partial A_{\mathrm{p}}^i}{\partial z} + \mathrm{Transport}\,, \tag{3}$$

Table 1. List of parameters, abbreviations and values.

Variable	Symbol	Value	Units
Production of ^{231}Pa from U decay	β^{Pa}	2.33×10^{-3}	$\mathrm{dpm\,m^{-3}\,yr^{-1}}$
Production of ^{230}Th from U decay	β^{Th}	2.52×10^{-2}	$\mathrm{dpm\,m^{-3}\,yr^{-1}}$
Decay constant of ^{231}Pa	λ^{Pa}	2.13×10^{-5}	$\mathrm{yr^{-1}}$
Decay constant of ^{230}Th	λ^{Th}	9.22×10^{-6}	$\mathrm{yr^{-1}}$
Index for ^{231}Pa and ^{230}Th	i		
Index for particle type	j		
Total isotope activity	A_{t}		$\mathrm{dpm\,m^{-3}}$
Dissolved isotope activity	A_{d}		$\mathrm{dpm\,m^{-3}}$
Particle associated activity	A_{p}		$\mathrm{dpm\,m^{-3}}$
Particle settling velocity	w_{s}	1000	$\mathrm{m\,yr^{-1}}$
Particle concentration	C		$\mathrm{kg\,m^{-3}}$
Density of seawater		1024.5	$\mathrm{kg\,m^{-3}}$
Ratio between particle concentration and density of seawater	R		

Table 2. Partition coefficients for different particle types and residence time for ^{231}Pa and ^{230}Th in different experiments.

	CTRL		Exp_1		Exp_2	
	^{231}Pa	^{230}Th	^{231}Pa	^{230}Th	^{231}Pa	^{230}Th
$K_{\mathrm{CaCO_3}}$	2.5×10^5	1.0×10^7	5×10^4	2×10^6	1.25×10^6	5×10^7
K_{opal}	1.67×10^6	5×10^5	3.33×10^5	1×10^5	8.33×10^6	2.5×10^6
K_{POC}	1.0×10^7	1.0×10^7	2×10^6	2×10^6	5×10^7	5×10^7
τ (yr)	118	33	501	143	27	9

Partition coefficients used in CTRL follows (Chase et al., 2002; Siddall et al., 2005). Both p-coupled and p-fixed versions are enabled in CTRL, which yields identical results (discussed in Sect. 4.1). Only the p-fixed version is enabled in Exp_1 and Exp_2. The residence time (τ) is for the p-fixed version in each experiment.

where the total isotope activity is controlled by decay from U (first term), radioactive decay (second term), reversible scavenging (third term) and physical transport by the ocean model (fourth term, including advection, convection and diffusion). A_{p}^i can be calculated by combining Eq. (1) and Eq. (2):

$$\begin{aligned} A_{\mathrm{t}}^i &= A_{\mathrm{d}}^i + A_{\mathrm{d}}^i \cdot \left(K_{\mathrm{POC}}^i \cdot R_{\mathrm{POC}} + K_{\mathrm{CaCO_3}}^i \cdot R_{\mathrm{CaCO_3}} + K_{\mathrm{opal}}^i \cdot R_{\mathrm{opal}}\right) \\ &= A_{\mathrm{d}}^i \cdot \left(1 + K_{\mathrm{POC}}^i \cdot R_{\mathrm{POC}} + K_{\mathrm{CaCO_3}}^i \cdot R_{\mathrm{CaCO_3}} + K_{\mathrm{opal}}^i \cdot R_{\mathrm{opal}}\right), \end{aligned} \tag{4}$$

which leads to

$$A_{\mathrm{d}}^i = \frac{A_{\mathrm{t}}^i}{1 + K_{\mathrm{POC}}^i \cdot R_{\mathrm{POC}} + K_{\mathrm{CaCO_3}}^i \cdot R_{\mathrm{CaCO_3}} + K_{\mathrm{opal}}^i \cdot R_{\mathrm{opal}}}. \tag{5}$$

When this is related back to Eq. (1), we get

$$A_{\mathrm{p}}^i = A_{\mathrm{t}}^i \cdot \left(1 - \frac{1}{1 + K_{\mathrm{POC}}^i \cdot R_{\mathrm{POC}} + K_{\mathrm{CaCO_3}}^i \cdot R_{\mathrm{CaCO_3}} + K_{\mathrm{opal}}^i \cdot R_{\mathrm{opal}}}\right). \tag{6}$$

Particle fields used in the reversible scavenging can be either prescribed or simultaneously generated from the marine ecosystem module. Therefore, two forms of ^{231}Pa and ^{230}Th are implemented in POP2: "p-fixed" and "p-coupled". The p-fixed ^{231}Pa and ^{230}Th use particle fluxes prescribed as annual mean particle fluxes generated from the marine ecosystem module under present-day climate forcing (Fig. 1). The p-coupled ^{231}Pa and ^{230}Th use particle fluxes computed simultaneously from the marine ecosystem module. The p-fixed and p-coupled ^{231}Pa and ^{230}Th can be turned on at the case build time and the p-coupled ^{231}Pa and ^{230}Th requires the ecosystem module to be turned on at the same time.

Compared with previous studies of modeling ^{231}Pa and ^{230}Th, our p-fixed version is the same as Siddall et al. (2005), except that different prescribed particle fluxes are used. The p-coupled version allows coupling to a biogeochemical module, which is similar to Rempfer et al. (2017), but we do not include boundary scavenging and sediment resuspensions as in Rempfer et al. (2017) because boundary scavenging and sediment resuspensions are suggested to be unimportant in influencing the relationship between $^{231}\mathrm{Pa_p}$ / $^{230}\mathrm{Th_p}$ and AMOC strength (Rempfer et al., 2017).

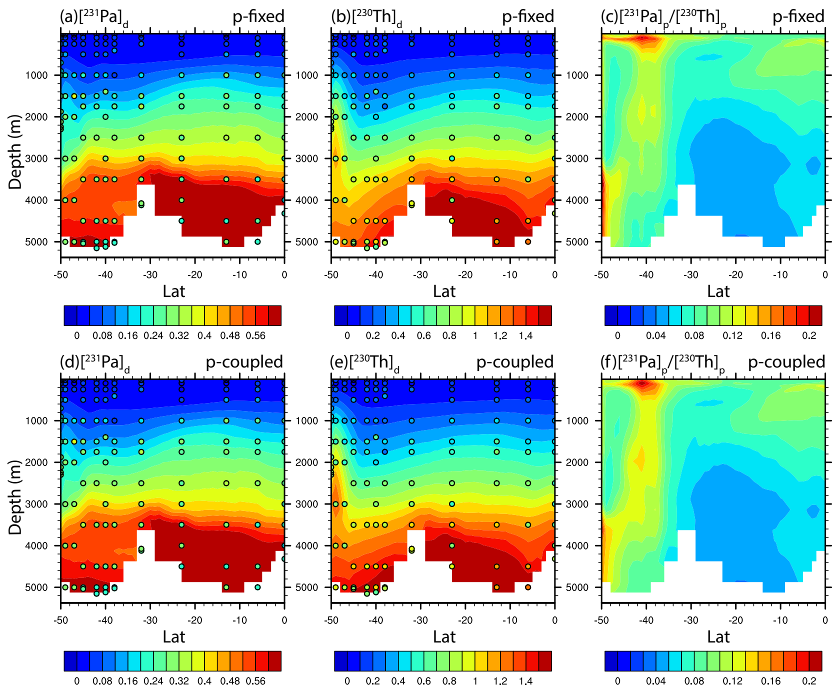

Figure 2. Dissolved ^{231}Pa, dissolved ^{230}Th and particulate ^{231}Pa / ^{230}Th in CTRL along GEOTRACES transect GA02S (Deng et al., 2014) (the track is indicated in Fig. S4 in the Supplement) for both p-fixed (top row) and p-coupled (bottom row) ^{231}Pa and ^{230}Th (colored contour). Observations of dissolved ^{231}Pa and ^{230}Th activity are superimposed as colored circles using the same color scale.

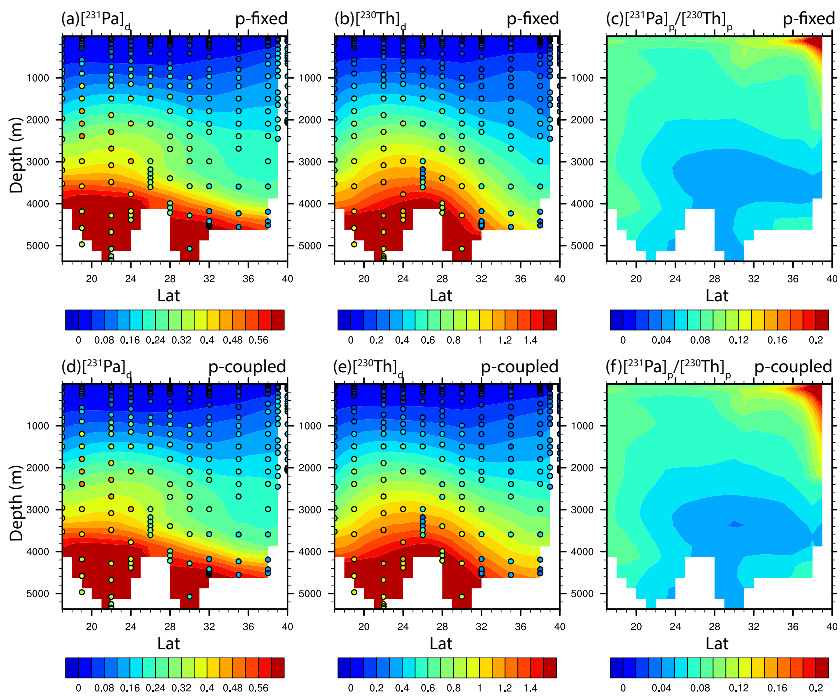

Figure 3. Dissolved ^{231}Pa, dissolved ^{230}Th and particulate ^{231}Pa / ^{230}Th in CTRL along GEOTRACES transect GA03 (Hayes et al., 2015) (the track is indicated in Fig. S4) for both p-fixed (top row) and p-coupled (bottom row) ^{231}Pa and ^{230}Th (colored contour). Observations of dissolved ^{231}Pa and ^{230}Th activity are superimposed as colored circles using the same color scale.

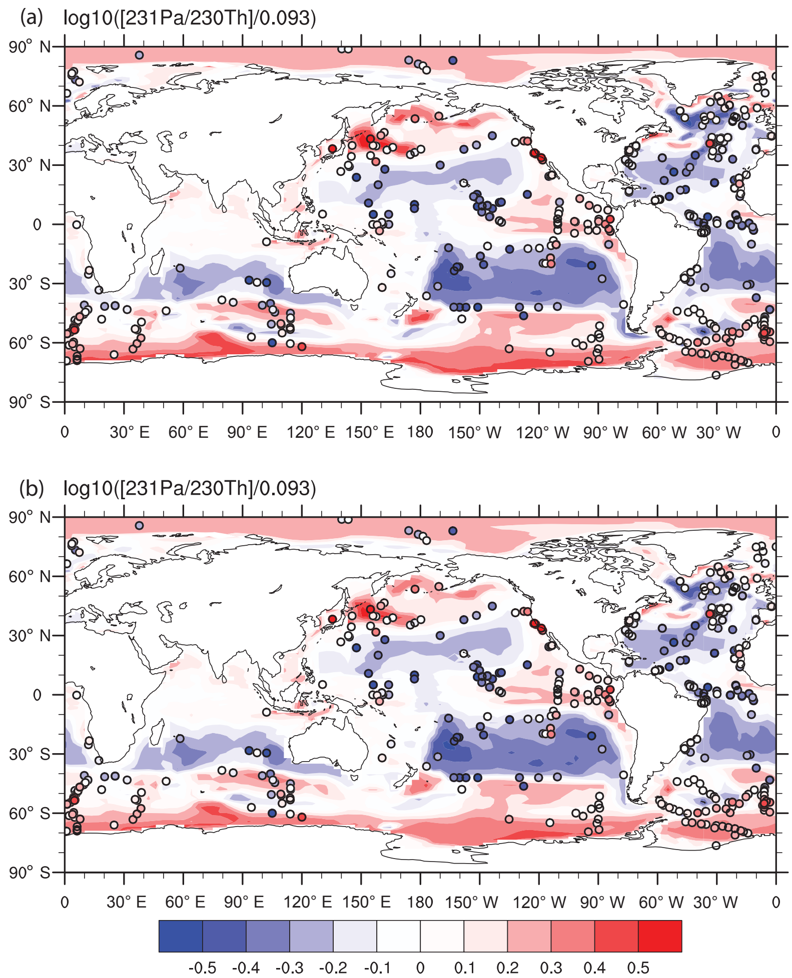

Figure 4. The sediment ^{231}Pa / ^{230}Th activity ratio in CTRL for both p-fixed **(a)** and p-coupled version **(b)**. Observations are attached as filled circles using the same color map. The ^{231}Pa / ^{230}Th activity ratio is plotted relative to the production ratio of 0.093 on a $\log_{10}$ scale.

3 Experiments

We run a control experiment (CTRL) and two experiments with different partition coefficients to show model sensitivity. We have both p-fixed and p-coupled ^{231}Pa and ^{230}Th in CTRL, but only p-fixed ^{231}Pa and ^{230}Th in sensitivity experiments. Equilibrium partition coefficients for ^{231}Pa and ^{230}Th vary among different particle types and the magnitude of the partition coefficients for different particle types remains uncertain (Chase et al., 2002; Chase and Robert, 2004; Luo and Ku, 1999). Since the control experiment in Siddall et al. (2005) is able to simulate major features of ^{231}Pa and ^{230}Th distributions, we use the partition coefficients from the control experiment in Siddall et al. (2005) in our CTRL (Table 2). Two sensitivity experiments are performed with decreased (EXP_1) and increased (EXP_2) partition coefficients by a factor of 5 (Table 2).

All the experiments are ocean-alone experiments with the normal year forcing by CORE-II data (Large and Yeager, 2008). The ^{231}Pa and ^{230}Th activities are initiated from 0 in CTRL and are integrated for 2000 model years until equilibrium is reached. EXP_1 and EXP_2 are initiated from model year 1400 in CTRL and are integrated for another 800 model years to reach equilibrium.

Since sediment ^{231}Pa / ^{230}Th in North Atlantic has been used to reflect the strength of AMOC, to test how sediment ^{231}Pa / ^{230}Th in our model responds to the change in AMOC and the change in particle fluxes, we carried out a freshwater perturbation experiment (HOSING) with both p-fixed and p-coupled ^{231}Pa and ^{230}Th. Starting from model year 2000 of CTRL, a freshwater flux of 1 Sv is imposed over the North Atlantic region of 50 to 70° N and the experiment is integrated for 1400 model years until both p-fixed and p-coupled sediment ^{231}Pa / ^{230}Th ratios have reached quasi-equilibrium. The partition coefficients used in HOSING are the same as in CTRL.

4 Results

4.1 Control experiment

P-fixed and p-coupled version of ^{231}Pa and ^{230}Th in CTRL show identical results (Figs. 2–4). The p-fixed and p-coupled dissolved and particulate ^{231}Pa and ^{230}Th in CTRL are highly correlated with each other, with correlations greater than 0.995, and regression coefficients are all near 1.0 ($R^2 > 0.995$). The correlation coefficient between p-fixed and p-coupled sediment ^{231}Pa / ^{230}Th activity ratios in CTRL is 0.99 and the regression coefficient is 0.9 ($R^2 = 0.98$). This is expected because the particle fields used in the p-fixed version are prescribed as the climatology of the particle fields used in the p-coupled version. Therefore, under the same climate forcing, p-fixed and p-coupled version of ^{231}Pa and ^{230}Th should be very similar. For the discussion of results in CTRL below, we only discuss the p-fixed ^{231}Pa and ^{230}Th.

The residence time of both ^{231}Pa and ^{230}Th in CTRL are comparable with observations. The residence time is calculated as the ratio of global-average total isotope activity and the radioactive ingrowth of the isotope. Residence time in CTRL is 118 yr for ^{231}Pa and 33 yr for ^{230}Th (Table 2), which are of the same magnitude as 111 yr for ^{231}Pa and 26 yr for ^{230}Th in observation (Yu et al., 1996).

CTRL can simulate the general features of dissolved water column ^{231}Pa and ^{230}Th activities. Dissolved ^{231}Pa and ^{230}Th activities increase with depth in CTRL, as shown in two GEOTRACES transects (Deng et al., 2014; Hayes et al., 2015) in the Atlantic (Figs. 2 and 3). The dissolved ^{231}Pa and ^{230}Th activities in CTRL are also of the same order of magnitude as in observations in most of the ocean, except that simulated values are larger than observations in the abyssal, which is also the case in Siddall et al. (2005) and Rempfer et al. (2017) (their Figs. 2 and 3, experiment Re3d). Our model is unable to simulate the realistic dissolved ^{231}Pa and ^{230}Th activities in the abyssal, probably because boundary scavenging and sediment resuspensions are not included in our model. In Rempfer et al. (2017), without boundary scavenging and sediment resuspension, dissolved ^{231}Pa and ^{230}Th activities are quite large in the deep ocean. However, if boundary scavenging and sediment resuspension are included, the water column dissolved ^{231}Pa and ^{230}Th activity is in the right magnitude compared with observation. Therefore, we hypothesize that with boundary scavenging and sediment resuspensions added, dissolved ^{231}Pa and ^{230}Th activities in the abyssal should be greatly reduced.

A more quantitative model–data comparison is shown in Fig. 5. The linear regression coefficient between model results and observations (references of observations are listed in Table 3), an indication of model ability to simulate ^{231}Pa and ^{230}Th activity (Dutay et al., 2009), is near 1.0 for dissolved ^{231}Pa and ^{230}Th (1.02 for $[^{231}\mathrm{Pa}]_\mathrm{d}$ and 1.14 for $[^{230}\mathrm{Th}]_\mathrm{d}$), suggesting that CTRL can simulate the dissolved ^{231}Pa and ^{230}Th in good agreement with observations. However, the simulation of the particulate activity is not as good as the dissolved activity. Particulate activity is overall larger than observation in the surface ocean and smaller than observation in the deep ocean for both particulate ^{231}Pa and ^{230}Th. The regression coefficient for particulate ^{231}Pa and ^{230}Th is 0.02 for $[^{231}\mathrm{Pa}]_\mathrm{p}$ and 0.05 for $[^{230}\mathrm{Th}]_\mathrm{p}$. The poor performance in simulating water column particulate ^{231}Pa and ^{230}Th activities is also in previous modeling studies (Dutay et al., 2009; Siddall et al., 2005), because of similar modeling schemes applied. However, the simulated $^{231}\mathrm{Pa}_\mathrm{p}$ / $^{230}\mathrm{Th}_\mathrm{p}$ is in reasonable agreement with observations. The $^{231}\mathrm{Pa}_\mathrm{p}$ / $^{230}\mathrm{Th}_\mathrm{p}$ along two GEOTRACES transects (Figs. 2 and 3) show the similar pattern and magnitude as in Rempfer et al. (2017), consistent with observations. Decrease of $^{231}\mathrm{Pa}_\mathrm{p}$ / $^{230}\mathrm{Th}_\mathrm{p}$ with depth is well simulated, which is suggested to be caused by the lateral transport

Table 3. References for observations of water column ^{231}Pa and ^{230}Th activity (left column) and Holocene core-top ^{231}Pa / ^{230}Th (right column).

Water column activity	Holocene core-top ^{231}Pa / ^{230}Th
Guo et al., 1995	Yu, 1994
Cochran et al., 1987	DeMaster, 1979
Nozaki et al., 1987	Bacon and Rosholt, 1982
Bacon and Anderson, 1982	Mangini and Diester-Hass, 1983
Bacon et al., 1989	Kumar, 1994
Huh and Beasley, 1987	Yang et al., 1986
Rutgers van der Loeff and Berger, 1993	Anderson et al., 1983
Nozaki et al., 1981	Anderson et al., 1994
Nozaki and Nakanishi, 1985	Ku, 1966
Mangini and Key, 1983	Ku et al., 1972
Nozaki and Horibe, 1983	Frank et al., 1994
Moore, 1981	Shimmield et al., 1986
Nozaki and Yamada, 1987	Frank, 1996
Roy-Barman et al., 1996	Yong Lao et al., 1992
Nozaki and Yang, 1987	Francois et al., 1993
Moran et al., 1995	Anderson et al., 1990
Luo et al., 1995	Mangini and Sonntag, 1977
Colley et al., 1995	Schmitz et al., 1986
Scholten et al., 1995	Shimmield and Price, 1988
Cochran et al., 1995	Yong-Liang Yang et al., 1995
Vogler et al., 1998	Müller and Mangini, 1980
Moran et al., 1997	Mangini and Kühnel, 1987
Edmonds et al., 1998	Scholten et al., 1995
Moran et al., 2001	Walter et al., 1997
Edmonds et al., 2004	Lippold et al., 2011
Okubo et al., 2007b	Lippold et al., 2012b
Coppola et al., 2006	Bradtmiller et al., 2007
Moran et al., 2002	Gherardi et al., 2005
Okubo et al., 2004	Gutjahr et al., 2008
Okubo et al., 2007a	Hall et al., 2006
Okubo et al., 2012	Lippold et al., 2011
Robinson et al., 2004	Roberts et al., 2014
Thomas et al., 2006	Bradtmiller et al., 2014
Trimble et al., 2004	Burckel et al., 2016
Venchiarutti et al., 2011	Hoffmann et al., 2013
Hsieh et al., 2011	Jonkers et al., 2015
Scholten et al., 2008	Negre et al., 2010
Luo et al., 2010	
Deng et al., 2014	
Hayes et al., 2013	
Hayes et al., 2015	

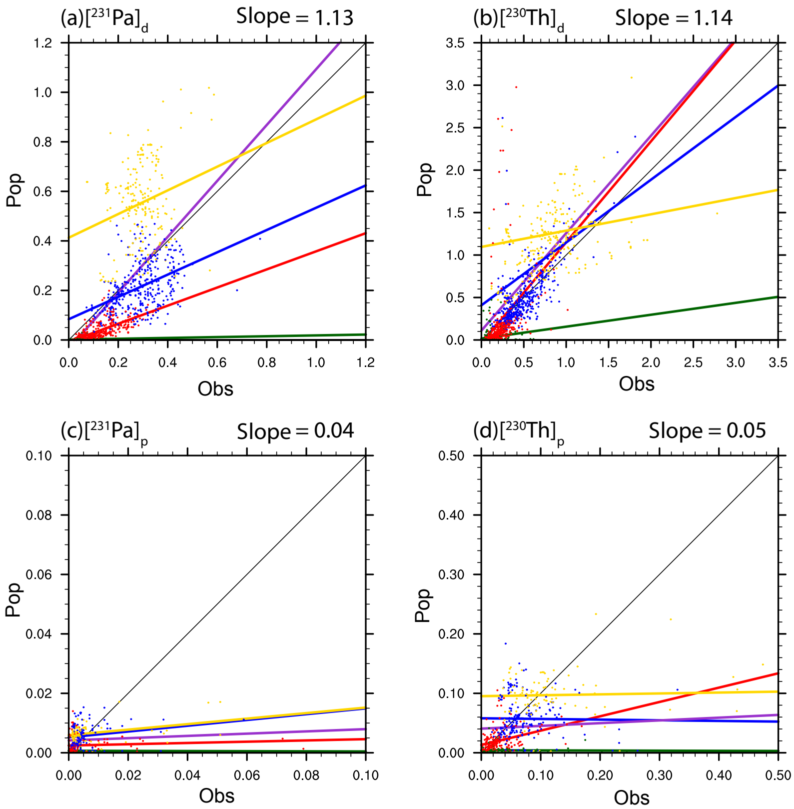

Figure 5. Scatter plot of global dissolved and particulate ^{231}Pa and ^{230}Th between observation and CTRL (p-fixed) (unit: dpm m^{-3}): **(a)** dissolved ^{231}Pa, **(b)** particulate ^{231}Pa, **(c)** dissolved ^{230}Th, **(d)** particulate ^{230}Th. Observations in different depth ranges are indicated by different colors: green for 0–100 m, red for 100–1000 m, blue for 1000–3000 m and yellow for deeper than 3000 m. The purple line is the least-squares linear regression line for all depth ranges, the slope of which is indicated at the top right of each plot. The green line is the least-squares linear regression line for depth from 0 to 100 m. The red line is the least-squares linear regression line for depth from 100 to 1000 m. The blue line is the least-squares linear regression line for depth from 1000 to 3000 m. The yellow line is the least-squares linear regression line for depth deeper than 3000 m.

of ^{231}Pa from the North Atlantic to the Southern Ocean by AMOC (Gherardi et al., 2009; Lippold et al., 2011, 2012a; Luo et al., 2010; Rempfer et al., 2017).

The sediment ^{231}Pa / ^{230}Th in CTRL is overall consistent with observations (references of observations are listed in Table 3). The North Atlantic shows a low sediment ^{231}Pa / ^{230}Th activity ratio as in observations because ^{231}Pa is more subject to the southward transport by active ocean circulation than ^{230}Th because of its longer residence time. The Southern Ocean maximum in the sediment ^{231}Pa / ^{230}Th activity ratio is also simulated in CTRL. High opal fluxes in the Southern Ocean, which preferentially removes ^{231}Pa into sediment ($K_{\mathrm{opal}}^{231\mathrm{Pa}} > K_{\mathrm{opal}}^{230\mathrm{Th}}$) (Chase et al., 2002), leading to an increased sediment ^{231}Pa / ^{230}Th activity ratio. In addition, upwelling in the Southern Ocean brings up deep water enriched with ^{231}Pa, which is transported from the North Atlantic, to shallower depth and further contributes to the scavenging. CTRL can also produce a higher sediment ^{231}Pa / ^{230}Th activity ratio in regions with high particle production (e.g., the eastern equatorial Pacific, the North Pacific and the Indian Ocean) due to the "particle flux effect". Specifically, in the North Atlantic, the distribution of sediment ^{231}Pa / ^{230}Th matches the distribution of particle, especially opal, production: sediment ^{231}Pa / ^{230}Th is higher where opal production is high, and vice versa (Fig. 4 and Fig. 1c). Quantitatively, the regression coefficient between sediment ^{231}Pa / ^{230}Th in CTRL and observation in the Atlantic is 0.86, which is larger than in other basins. This suggests that sediment ^{231}Pa / ^{230}Th is better simulated in the Atlantic than in other basins. One possible explanation is that sediment ^{231}Pa / ^{230}Th in the Atlantic is controlled by both ocean circulation and particle flux, while in other basins sediment ^{231}Pa / ^{230}Th is controlled almost only by particle flux. With active AMOC, the north–south gradient of sediment ^{231}Pa / ^{230}Th can be simulated. However, for example, in the Southern Ocean, sediment ^{231}Pa / ^{230}Th is dominantly controlled by opal flux, which varies on small scales and is difficult for simulation. Therefore, model performance in simulating sediment ^{231}Pa / ^{230}Th in the Southern Ocean is not as good as in the Atlantic.

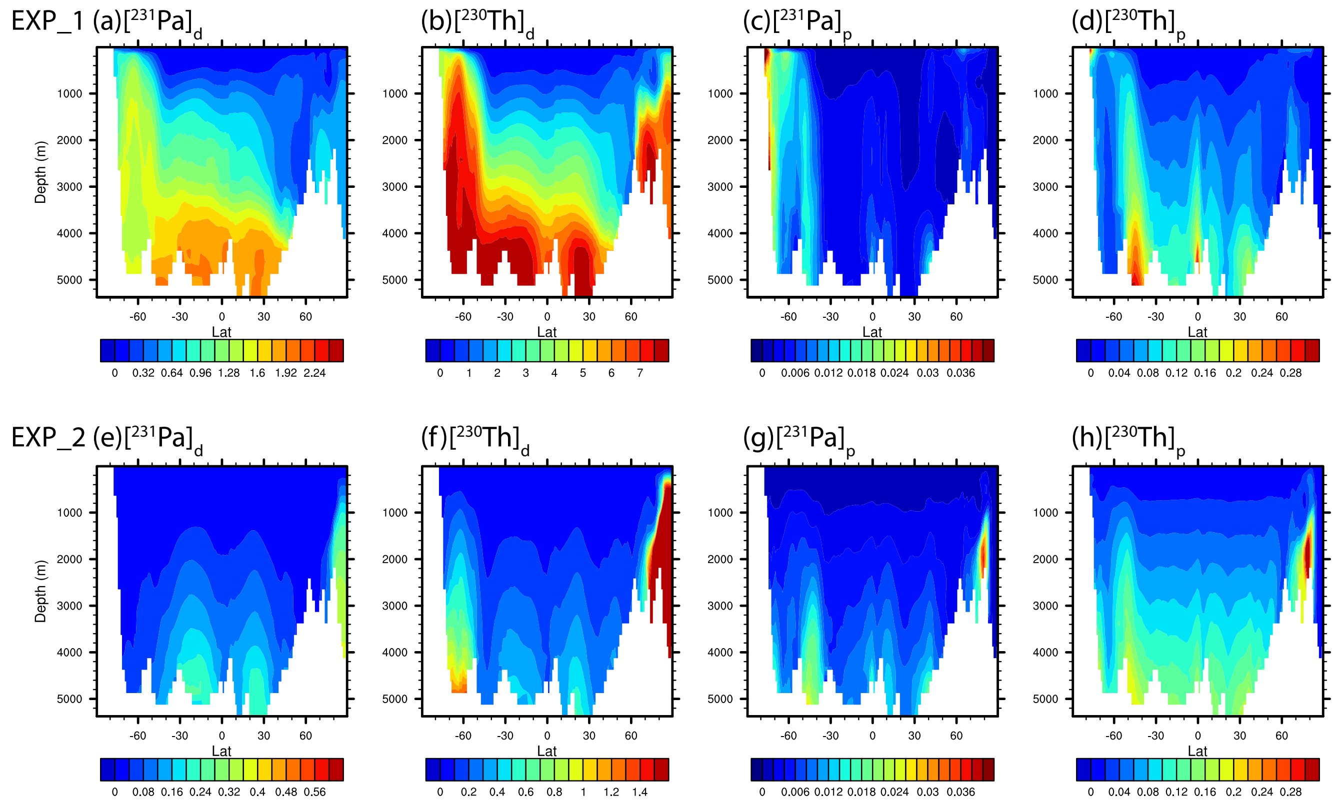

Figure 6. Atlantic zonal mean dissolved and particulate ^{231}Pa and ^{230}Th in Exp_1 and Exp_2 (unit: dpm m^{-3}). Exp_1: **(a)** dissolved ^{231}Pa, **(b)** dissolved ^{230}Th, **(c)** particulate ^{231}Pa, **(d)** particulate ^{230}Th. Exp_2: **(e)** dissolved ^{231}Pa, **(f)** dissolved ^{230}Th, **(g)** particulate ^{231}Pa, **(h)** particulate ^{230}Th.

4.2 Sensitivity to partition coefficient K

In this section, we show model sensitivity to partition coefficients by increasing and decreasing the partition coefficient, K, by a factor of 5, but keeping the relative ratio for different particles the same (Table 2). Our model shows similar model sensitivity as in Siddall et al. (2005) as discussed below.

As stated in Siddall et al. (2005), the isotope decay term in Eq. (3) is 3 orders of magnitude less than the production term. If we neglect the transport term and the decay term in Eq. (3) and assume particulate phase activity at the surface as 0, when equilibrium is reached, the activity of particulate phase will be as in Eq. (7). By combining Eq. (7) with Eq. (2) and $R_i = \frac{F}{w_s \cdot \rho}$, we can obtain Eq. (8). Under the assumption that there is isotope decay and ocean transport, Eq. (7) suggests that the particulate isotope activity depends on the production rate and settling velocity and will increase linearly with depth. Equation (8) suggests that the dissolved isotope activity depends on the production rate, partition coefficient K and particle flux and will also increase linearly with depth. Any departure from this linear relationship with depth is due to ocean transport, which is suggested by observations (Bacon and Anderson, 1982; Roy-Barman et al., 1996). Results of Eqs. (7) and (8) can aid understanding of the differences in Exp_1 and Exp_2.

Increasing K will decrease water column dissolved ^{231}Pa and ^{230}Th activities but will not change particulate ^{231}Pa and ^{230}Th too much (Fig. 6). Magnitude of dissolved ^{231}Pa and ^{230}Th in Exp_1 (smaller K) is at least 1 order larger than that in Exp_2 (larger K), while magnitude of particulate ^{231}Pa and ^{230}Th in Exp_1 and Exp_2 is of the same order. As suggested by Eq. (8), if there is no isotope decay and no ocean transport, larger K will lead to smaller dissolved isotope activity but unchanged particulate activity. Intuitively, larger K will lead to more ^{231}Pa and ^{230}Th attached to particles and further buried into sediment, which increases the sink for the ^{231}Pa and ^{230}Th budget. With the sources for ^{231}Pa and ^{230}Th staying the same, dissolved ^{231}Pa and ^{230}Th will be reduced. Increasing K will also reduce the vertical gradient of dissolved ^{231}Pa and ^{230}Th, because reversible scavenging acts as the vertical transport and increases this vertical transport and can also decrease the vertical gradient. However, changes in the particulate ^{231}Pa and ^{230}Th are relatively small (Fig. 6). Equation (7) suggests that particulate phase activity is independent of K. Therefore, changing K will have limited influence on particulate phase activity.

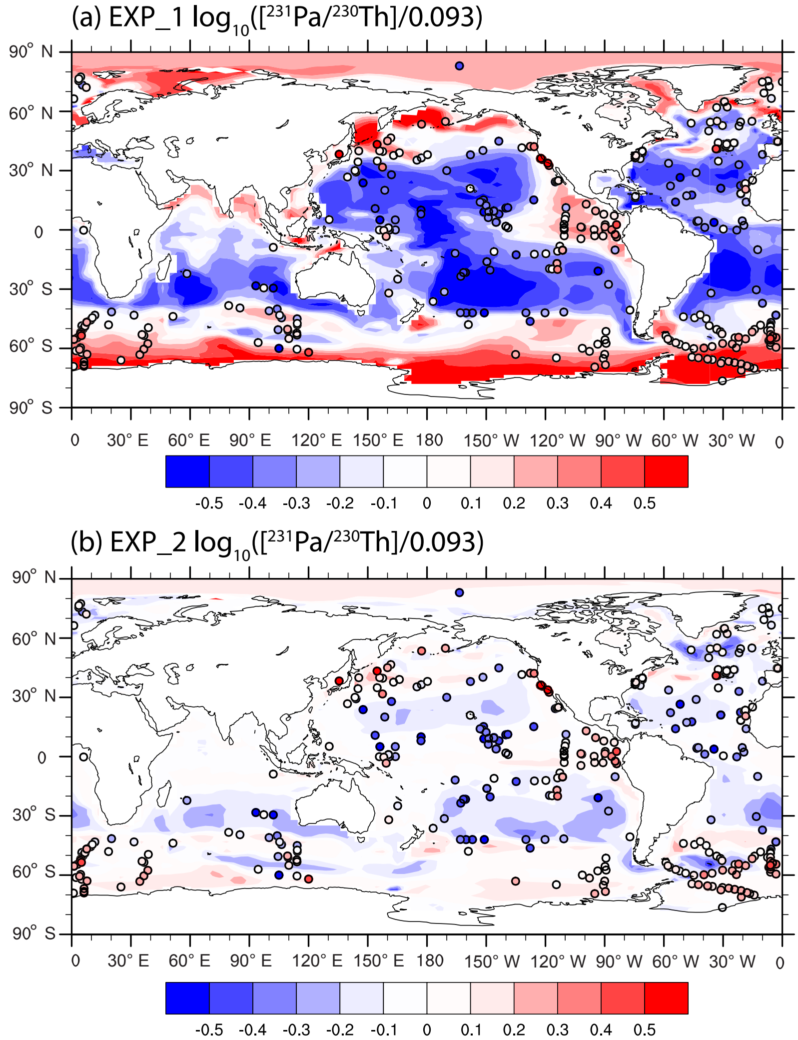

Figure 7. The sediment ^{231}Pa / ^{230}Th activity ratio in Exp_1 **(a)** and Exp_2 **(b)**. Observations are attached as filled circles using the same color map. The ^{231}Pa / ^{230}Th activity ratio is plotted relative to the production ratio of 0.093 on a $\log_{10}$ scale.

$$A_p^i(z) = \frac{\beta^i}{w_s} \cdot z \tag{7}$$

$$A_d^i(z) = \frac{\rho \beta^i}{K^i F} \cdot z \tag{8}$$

Increasing K will also reduce the spatial gradient in the sediment ^{231}Pa / ^{230}Th activity ratio and vice versa (Fig. 7). Larger K will decrease the ^{231}Pa and ^{230}Th residence time and most isotopes produced in the water column are removed into sediment locally (Table 2). Therefore, the sediment ^{231}Pa / ^{230}Th ratio becomes more homogeneous and approaching the production ration of 0.093 (Fig. 7b). The deviation (the root mean squared error) of sediment ^{231}Pa / ^{230}Th is 0.0726 in CTRL, 0.0770 in Exp_1 and 0.0739 in Exp_2. The linear regression coefficients between sediment ^{231}Pa / ^{230}Th in the model and the observations are listed in Table S1 in the Supplement. Although the performance of global sediment ^{231}Pa / ^{230}Th in Exp_1 is better than CTRL, the performance of Atlantic ^{231}Pa / ^{230}Th in Exp_1 is worse. We consider better simulation of sediment ^{231}Pa / ^{230}Th in the Atlantic to be more important since the most important application of sediment ^{231}Pa / ^{230}Th is using sediment ^{231}Pa / ^{230}Th in the North Atlantic to reconstruct past AMOC. In addition, water column isotope activity is too large in Exp_1 compared with observations. Therefore, the partition coefficient in CTRL is of the right order of magnitude.

4.3 The sediment ^{231}Pa / ^{230}Th ratio in HOSING

Potential changes in the export of biogenic particles makes using the ^{231}Pa / ^{230}Th ratio to reconstruct AMOC strength a subject for debate. In response to freshwater perturbation in the North Atlantic, both biological productivity and

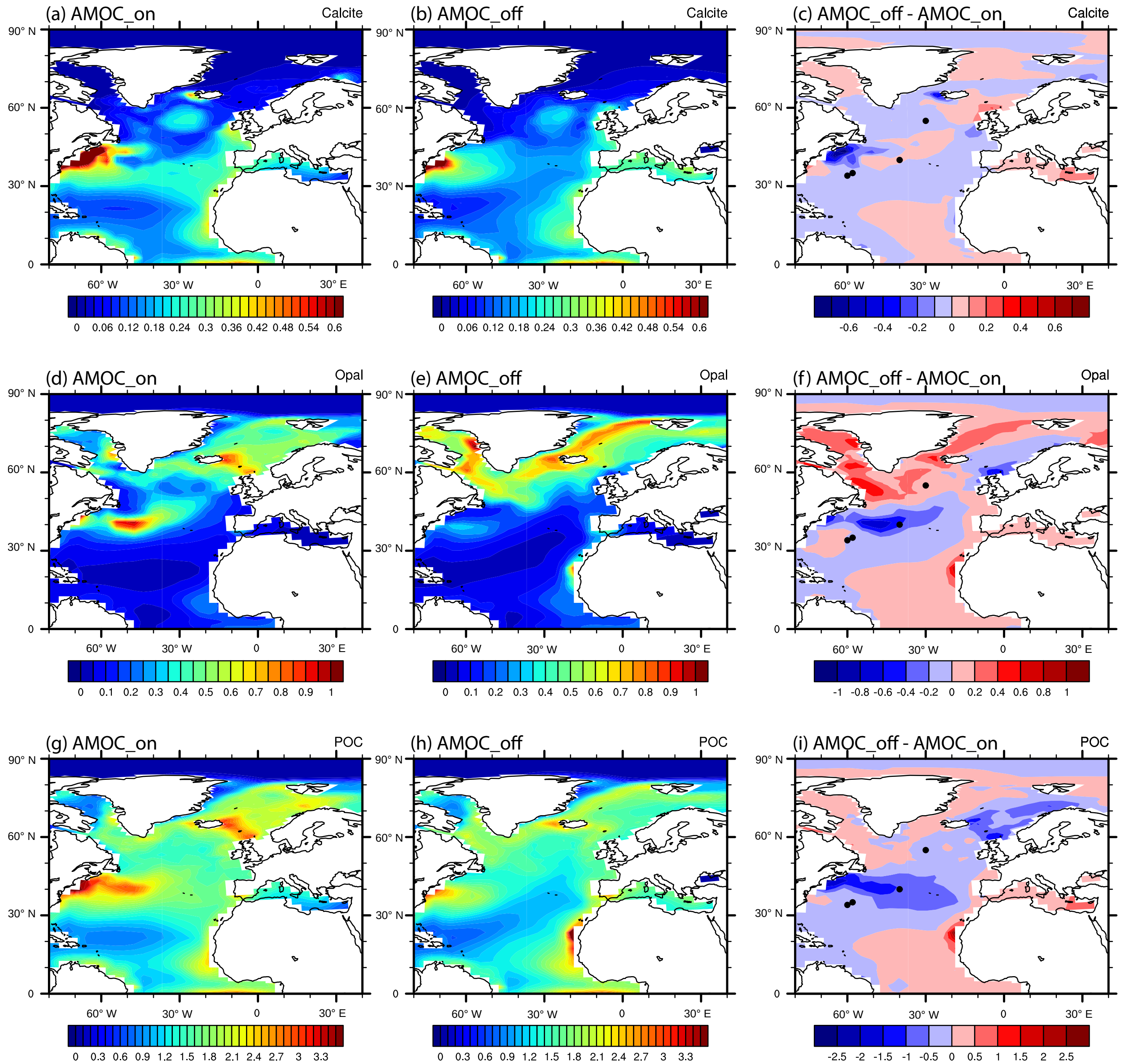

Figure 8. Comparison of particle fluxes between AMOC_on and AMOC_off. $CaCO_3$ flux at 105 m (mol m^{-2} yr^{-1}) during AMOC_on **(a)**, AMOC_off **(b)** and the difference between AMOC_off and AMOC_on. **(b)** Opal flux at 105 m (mol m^{-2} yr^{-1}) during AMOC_on **(d)**, AMOC_off **(e)** and the difference between AMOC_off and AMOC_on **(f)**. POC flux at 105 m (mol m^{-2} yr^{-1}) during AMOC_on **(g)**, AMOC_off **(h)** and the difference between AMOC_off and AMOC_on **(i)**.

AMOC strength will change and will influence sediment ^{231}Pa / ^{230}Th in different ways. Our model with p-fixed and p-coupled ^{231}Pa and ^{230}Th can help to detangle these two effects. In this section, we examine the sediment ^{231}Pa / ^{230}Th (p-fixed and p-coupled) response in the North Atlantic to idealized freshwater perturbation.

In HOSING, after applying freshwater forcing to the North Atlantic, AMOC strength quickly decreases to a minimum of 2 Sv (AMOC_off) (Fig. 9a). During the AMOC_off state, compared with CTRL with active AMOC (AMOC_on), p-fixed sediment ^{231}Pa / ^{230}Th shows an overall increase in the North Atlantic and a decrease in the South Atlantic (Fig. 10b) because of the reduced southward transport of ^{231}Pa from the North Atlantic by AMOC, consistent with paleo-proxy evidence there (e.g., Gherardi et al., 2005, 2009; McManus et al., 2004). The overall increase of the sediment ^{231}Pa / ^{230}Th ratio in the North Atlantic in response to the AMOC collapse can be seen more clearly in the time evolution of the sediment ^{231}Pa / ^{230}Th ratio averaged from 20 to 60° N in the North Atlantic (Fig. 9b, green). Quantitatively, the ^{231}Pa / ^{230}Th increases from 0.074 in AMOC_on to 0.098 in AMOC_off in the p-fixed version, approaching the production ration of 0.093. This increase of ^{231}Pa / ^{230}Th is also observed in the subtropical North Atlantic from the two sites near the Bermuda Rise (Fig. 9e and f), which is of comparable magnitude with the change from LGM to HS1 in reconstructions there (McManus et al., 2004). In addition, the pattern of the p-fixed (Fig. 10a) sediment ^{231}Pa / ^{230}Th ratio in the Atlantic in AMOC_off state is similar to the opal distribution (Fig. 1b) because, without active circulation, the sediment ^{231}Pa / ^{230}Th ratio is more controlled by particle flux effect, which is similar to the Pacific in CTRL. It is further noted that our p-fixed sediment ^{231}Pa / ^{230}Th ratio in HOSING behaves similarly to that in Siddall et al. (2007).

The overall increase in the p-fixed sediment ^{231}Pa / ^{230}Th ratio in the North Atlantic is not homogenous and the magnitude of the change between AMOC_on and AMOC_off varies with location depending on the distribution of particle flux, especially the opal flux (Figs. 9 and 10). The maximum increase in the p-fixed sediment ^{231}Pa / ^{230}Th ratio occurs near 40° N in the western Atlantic (Fig. 10a), where the opal production in our model is maximum in the North Atlantic (Fig. 1b). The sediment ^{231}Pa / ^{230}Th ratio in this region during AMOC_on is larger than the production ratio of 0.093 because opal maximum provides extra ^{231}Pa to this region ("particle flux effect"), which overwhelms the active ocean circulation transporting ^{231}Pa southward outside this region (Fig. 9d, green). During AMOC_off, without active ocean circulation, the particle flux effect becomes even stronger because less ^{231}Pa is transported out of the North Atlantic and the p-fixed sediment ^{231}Pa / ^{230}Th ratio becomes even larger. It should be noted that the opal maximum in this region is not in the observation (Fig. 7.2.5 in Sarmiento and Gruber, 2006). However, our sediment ^{231}Pa / ^{230}Th response in HOSING is self-consistent with the particle flux in our model since the location of the maximum ^{231}Pa / ^{230}Th increase matches the location of opal flux in our model.

In most regions of the Atlantic, p-coupled sediment ^{231}Pa / ^{230}Th shows a similar response to p-fixed ^{231}Pa / ^{230}Th in HOSING. The evolutions of p-fixed and p-coupled sediment ^{231}Pa / ^{230}Th activity ratios in HOSING are highly correlated (Fig. 11a). The change in the sediment ^{231}Pa / ^{230}Th ratio from AMOC_on to AMOC_off are similar in both the p-fixed and p-coupled version (Fig. 11b). The correlation between p-fixed and p-coupled sediment ^{231}Pa / ^{230}Th ratio change from AMOC_on to AMOC_off is 0.72 (1455 points) and the linear regression coefficient is 0.71 ($R^2 = 0.52$). A high correlation between p-fixed and p-coupled response mainly happens over low-productivity regions (Figs. 1, 10, and 11), where the circulation effect on

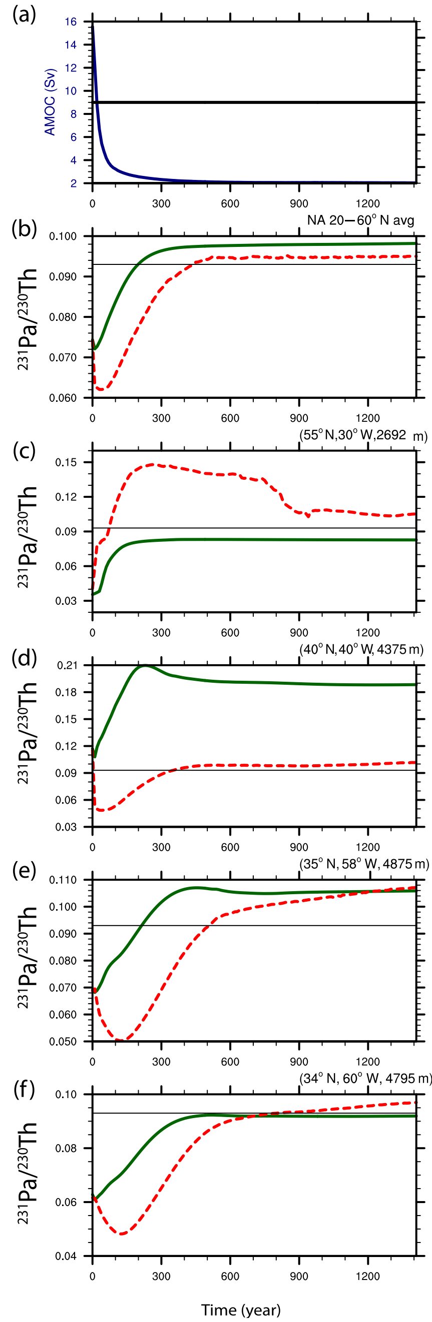

Figure 9. Time evolutions in HOSING. **(a)** Freshwater forcing (black) and AMOC strength (navy), which is defined as the maximum of the overturning stream function below 500m in the North Atlantic. **(b)** The North Atlantic average sediment ^{231}Pa / ^{230}Th activity ratio from 20° N to 60° N: p-fixed (green) and p-coupled (red). The production ratio of 0.093 is indicated by a solid black line (similar to in **c**, **d**, **e** and **f**). **(c)** The sediment ^{231}Pa / ^{230}Th activity ratio at (55° N, 30° W). **(d)** The sediment ^{231}Pa / ^{230}Th activity ratio at (40° N, 40° W). **(e)** The sediment ^{231}Pa / ^{230}Th activity ratio at (35° N, 58° W). **(f)** The sediment ^{231}Pa / ^{230}Th activity ratio at (34° N, 60° W). Panels **(e)** and **(f)** show locations near the Bermuda Rise. Locations of each site are shown as dots in Fig. 8b.

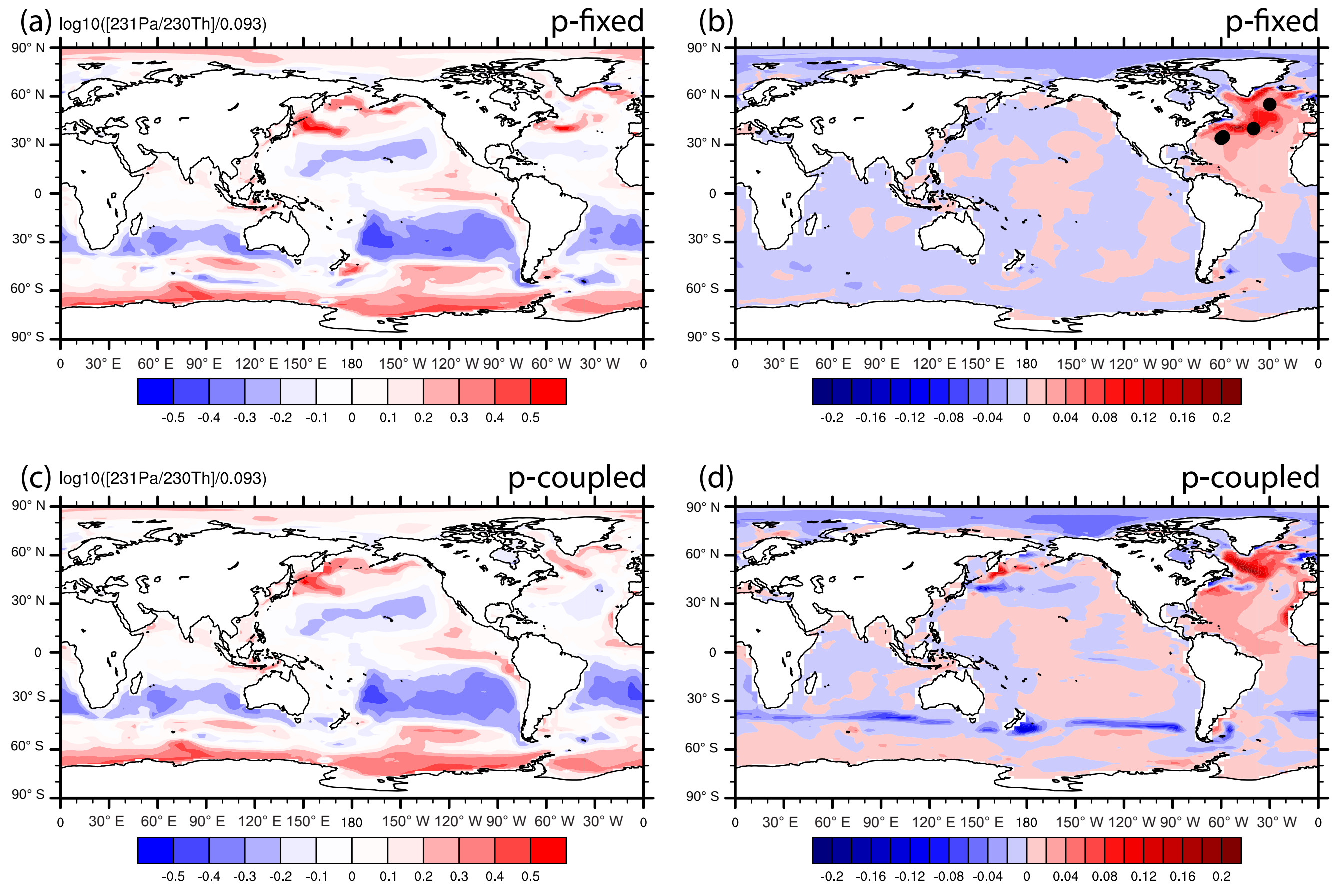

Figure 10. The sediment ^{231}Pa / ^{230}Th activity ratio during AMOC off state and the difference between AMOC off and CTRL. **(a)** P-fixed $\log_{10}([^{231}\mathrm{Pa}/^{230}\mathrm{Th}]/0.093)$ in AMOC_off. **(b)** Difference in the p-fixed sediment ^{231}Pa / ^{230}Th activity ratio between AMOC_off and AMOC_on. Panels **(c)** and **(d)** are similar to **(a)** and **(b)** for the p-coupled sediment ^{231}Pa / ^{230}Th activity ratio. Black dots in **(b)** shows the locations of sites in Fig. 9 from north to south.

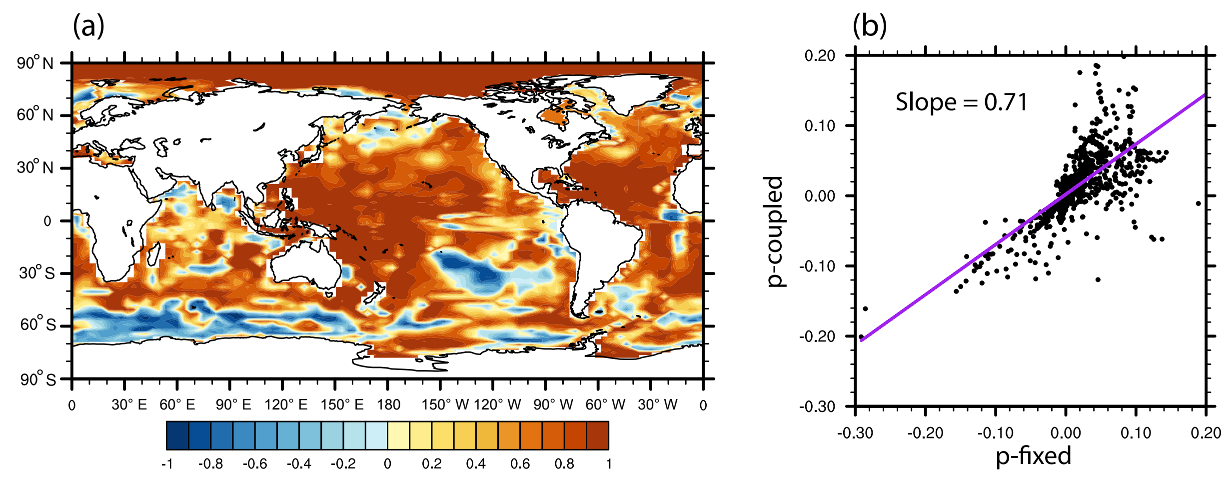

Figure 11. (a) Correlation of p-fixed and p-coupled evolution of the sediment ^{231}Pa / ^{230}Th activity ratio in HOSING. **(b)** Scatter plot of the p-fixed and p-coupled sediment ^{231}Pa / ^{230}Th activity ratio change from AMOC_on to AMOC_off in the Atlantic and the Southern Ocean (70° W–20° E). Purple line is the least-squares linear regression line and slope is the linear regression coefficient.

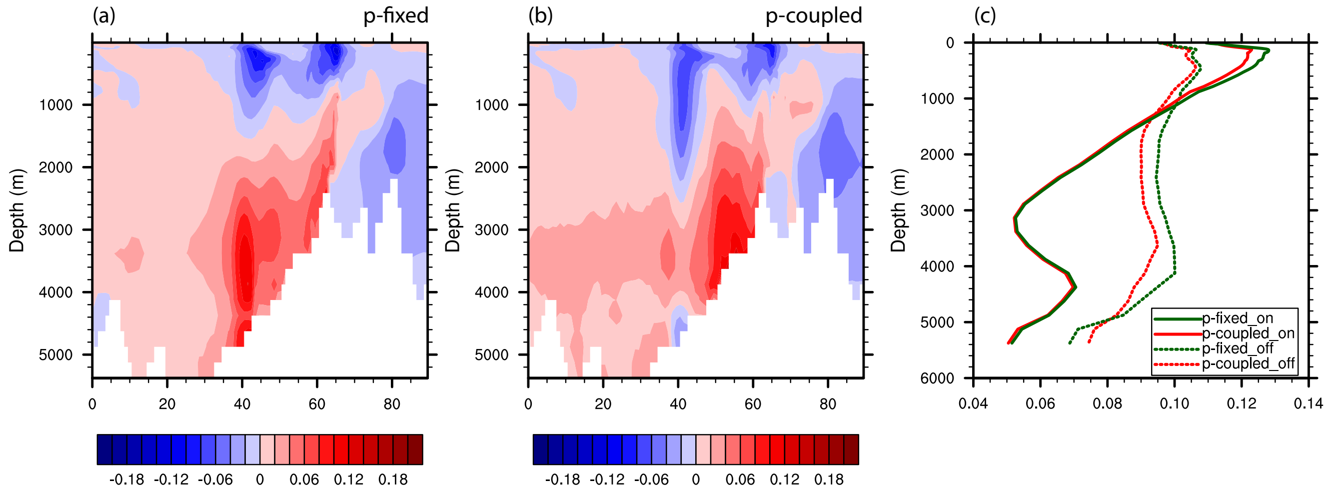

Figure 12. Difference of Atlantic zonal mean **(a)** p-fixed and **(b)** p-coupled particulate ^{231}Pa / ^{230}Th between AMOC_off and AMOC_on. **(c)** North Atlantic (20–60° N) average profile during AMOC_on (solid) and AMOC_off (dash) for p-fixed (green) and p-coupled (red) particulate ^{231}Pa / ^{230}Th.

sediment ^{231}Pa / ^{230}Th is more important than the particle flux change in HOSING.

In spite of these similarities discussed above, the responses of p-fixed and p-coupled sediment ^{231}Pa / ^{230}Th to the freshwater forcing can differ significantly in high-productivity regions because of the productivity change. With persistent freshwater forcing over the North Atlantic, most regions in the North Atlantic show reduced production of $CaCO_3$, opal and POC (Fig. 8). Productivity in the North Atlantic is suggested to be halved during AMOC collapse because of increased stratification, which reduces nutrient supply from the deep ocean (Schmittner, 2005). In our model, the productivity in the midlatitude North Atlantic is indeed greatly reduced after the freshwater forcing is applied. For example, opal production from 30 to 50° N in the Atlantic at the end of HOSING is reduced by 50–90 % of its original value in CTRL. However, opal production increases in the high-latitude North Atlantic (north of 50° N). The pattern of opal production changes with high-opal-production regions shifting northward in HOSING (Fig. 8d, e and f). These particle flux changes will influence sediment ^{231}Pa / ^{230}Th as discussed below.

North of 50° N in the Atlantic, opal productivity increases during AMOC_off (Fig. 8f) and will result an increase in sediment ^{231}Pa / ^{230}Th. The increase caused by greater opal productivity enhances the sediment ^{231}Pa / ^{230}Th increase caused by reduced AMOC. Therefore, the increase in p-coupled sediment ^{231}Pa / ^{230}Th from AMOC_on to AMOC_off is larger than p-fixed sediment ^{231}Pa / ^{230}Th change (Fig. 9c).

In the midlatitude North Atlantic, opal productivity decreases during AMOC_off (Fig. 8f) and will lead to a decrease in sediment ^{231}Pa / ^{230}Th, which is opposite to the effect of reduced AMOC. The p-coupled sediment ^{231}Pa / ^{230}Th shows an initial decrease in first 200 years (Fig. 9d, e and f, red dash lines) caused by the reduced opal productivity. But this decreasing trend is reversed eventually, suggesting that the influence of particle flux change is overwhelmed by the effect of reduced AMOC. It the long run, most regions in the subtropical and midlatitude Atlantic show increased sediment ^{231}Pa / ^{230}Th in HOSING (Fig. 10d), indicating the dominant effect of reduced AMOC. However, sediment ^{231}Pa / ^{230}Th at 40° N west Atlantic, where opal productivity is at its maximum during AMOC_on, show a decrease from AMOC_on to AMOC_off (Figs. 9d and 10d). During AMOC_on, the opal productivity maximum at 40° N in the west Atlantic lead to regional maximum sediment ^{231}Pa / ^{230}Th because of the particle flux effect (Fig. 4). During AMOC_off, this opal productivity maximum is eliminated (Fig. 8e) and there is no more extra ^{231}Pa supplied by surroundings to this region, which leads to a decrease in sediment ^{231}Pa / ^{230}Th. This decrease in sediment ^{231}Pa / ^{230}Th caused by productivity change is greater than the increase caused by the reduced AMOC. Therefore, sediment ^{231}Pa / ^{230}Th experiences a decrease from AMOC_on to AMOC_off at this location (Fig. 9d and Fig. 10d). Our results suggest that although the circulation effect is more dominant than the particle flux change in controlling sediment ^{231}Pa / ^{230}Th on long timescales over most of North Atlantic (Fig. 11), particle flux change can be important on short timescales and in high-productivity regions. With p-fixed and p-coupled ^{231}Pa and ^{230}Th, our model can help to detangle the circulation effect and particle flux effect.

It has been suggested that the particulate ^{231}Pa / ^{230}Th response to the change in AMOC depends on the location and depth. Above 2 km and high-latitude North Atlantic, particulate ^{231}Pa / ^{230}Th decreases with the increased AMOC (Rempfer et al., 2017). Our results are consistent with this finding (Fig. 12a and b). Both p-fixed and p-coupled particulate ^{231}Pa / ^{230}Th show similar patterns of change from AMOC_on to AMOC_off: a decrease in particulate ^{231}Pa / ^{230}Th at shallow depth and north of 60° N and an increase in particulate ^{231}Pa / ^{230}Th below 2 km and south of 60° N during AMOC_off. Therefore, sediment depth should also be taken into consideration when interpreting sediment ^{231}Pa / ^{230}Th. Since the pattern in the p-coupled ratio is similar to the pattern in the p-fixed ratio, the opposite particulate ^{231}Pa / ^{230}Th changes in the shallow and deep North Atlantic is associated with AMOC change. During AMOC_on, upper limb of AMOC (about upper 1 km) transport water northward, which provides extra ^{231}Pa to North Atlantic, and particulate ^{231}Pa / ^{230}Th is larger than the production ratio of 0.093. In contrast, the lower limb of AMOC (2–3 km) features southward transport, which transports ^{231}Pa to the Southern Ocean, and particulate ^{231}Pa / ^{230}Th is smaller than the production ratio of 0.093 (Fig. 12 solid). Particulate ^{231}Pa / ^{230}Th decreases with depth (Fig. 12c solid). During AMOC_off, ocean transport of ^{231}Pa is greatly reduced. Therefore, shallow (deep) depth experiences a decrease (increase) in particulate ^{231}Pa / ^{230}Th and the vertical gradient in the particulate ^{231}Pa / ^{230}Th is also greatly reduced (Fig. 12c dash). Our results support that the depth dependence of particulate ^{231}Pa / ^{230}Th is mainly caused by lateral transport of ^{231}Pa by circulation (Gherardi et al., 2009; Lippold et al., 2011, 2012a; Luo et al., 2010; Rempfer et al., 2017).

Overall, our model is able to simulate the correct magnitude of the sediment ^{231}Pa / ^{230}Th ratio response to the freshwater forcing. Our experiments suggest that the change in circulation is the dominant factor that influences sediment ^{231}Pa / ^{230}Th on long timescales over most of the globe in the idealized hosing experiment, although the detailed difference between p-fixed and p-coupled sediment ^{231}Pa / ^{230}Th ratio response to freshwater forcing in different locations can be complicated.

5 Summary

^{231}Pa and ^{230}Th have been implemented in the ocean model of the CESM in both the p-coupled and p-fixed forms. Our control experiment under present-day climate forcing is able to simulate most ^{231}Pa and ^{230}Th water column activity and the sediment ^{231}Pa / ^{230}Th activity ratio consistently with observations by using the parameters that are suggested by Chase et al. (2002) and used in Siddall et al. (2005). Our sensitivity experiments with varying parameters suggest that these parameters are of the right order of magnitude.

Furthermore, our model is able to simulate the overall sediment ^{231}Pa / ^{230}Th ratio change in the North Atlantic with a magnitude comparable to the reconstruction in response to the collapse of AMOC, although the detailed response can be complicated in different regions. Finally, the p-fixed form is able to capture many major features of that of the p-coupled form over large ocean areas on long timescales, although the two forms can also differ significantly in some regions, especially the region with high opal productivity.

Much remains to be improved in our ^{231}Pa and ^{230}Th module in the future. For example, the model can be further improved by including nepheloid layers to better simulate water column ^{231}Pa and ^{230}Th activity as in Rempfer et al. (2017). In addition, a partition coefficient for different particles can be further tuned, which can improve our understanding of the affinity of ^{231}Pa and ^{230}Th to different particles, complementing the limited observational studies available (e.g., Chase et al., 2002; Scholten et al., 2005; Walter et al., 1997). At present, as the first attempt to implement ^{231}Pa and ^{230}Th in the CESM with both p-fixed and p-coupled versions, our model can serve as a useful tool to improve our understanding of the processes of ^{231}Pa and ^{230}Th as well as interpretations of sediment ^{231}Pa / ^{230}Th reconstructions for past ocean circulation and climate changes.

Code availability. The ^{231}Pa and ^{230}Th isotope source code of both p-fixed and p-coupled versions for CESM1.3 is included in the Supplement.

Data availability. Data used to produce the results in this study can be obtained from HPSS at CISL (/home/sgu28/csm/PaTh_data) and is available on request to the author at sgu28@wisc.edu.

The Supplement related to this article is available online at https://doi.org/10.5194/gmd-10-4723-2017-supplement.

Competing interests. The authors declare that they have no conflict of interest.

Acknowledgements. This work is supported by NSF P2C2 program (NSF 1401778 and NSF1600080), DOE DE-SC0006744 and NSFC 41630527 and 41130105. Computing resources (ark:/85065/d7wd3xhc) were provided by the Climate Simulation Laboratory at NCAR's Computational and Information Systems Laboratory, sponsored by the National Science Foundation and other agencies. We thank Paul Halloran for serving as editor and three anonymous reviewers for their constructive comments on the discussion paper.

Edited by: Paul Halloran
Reviewed by: three anonymous referees

References

Anderson, R. F., Bacon, M. P., and Brewer, P. G.: Removal of ^{230}Th and ^{231}Pa from the open ocean, Earth Planet. Sc. Lett., 62, 7–23, https://doi.org/10.1016/0012-821X(83)90067-5, 1983.

Anderson, R. F., Lao, Y., Broecker, W. S., Trumbore, S. E., Hofmann, H. J., and Wolfli, W.: Boundary scavenging in the Pacific Ocean: A comparison of ^{10}Be and ^{231}Pa, Earth Planet. Sc. Lett., 96, 287–304, https://doi.org/10.1016/j.cognition.2008.05.007, 1990.

Anderson, R. F., Fleisher, M. Q., Biscaye, P. E., Kumar, N., Dittrich, B., Kubik, P., and Suter, M.: Anomalous boundary scavenging in the Middle Atlantic Bight: evidence from ^{230}Th, ^{231}Pa, ^{10}Be and ^{210}Pb, Deep-Sea Res. Pt. II, 41, 537–561, https://doi.org/10.1016/0967-0645(94)90034-5, 1994.

Armstrong, R. A., Lee, C., Hedges, J. I., Honjo, S., and Wakeham, S. G.: A new, mechanistic model for organic carbon fluxes in the ocean based on the quantitative association of POC with ballast minerals, Deep-Sea Res. Pt. II, 49, 219–236, https://doi.org/10.1016/S0967-0645(01)00101-1, 2002.

Arsouze, T., Dutay, J.-C., Lacan, F., and Jeandel, C.: Reconstructing the Nd oceanic cycle using a coupled dynamical – biogeochemical model, Biogeosciences, 6, 2829–2846, https://doi.org/10.5194/bg-6-2829-2009, 2009.

Bacon, M. P. and Anderson, R. F.: Distribution of Thorium Isotopes between dissolved and particulate forms in the deep sea, J. Geophys. Res.-Oceans, 87, 2045–2056, https://doi.org/10.1029/JC087iC03p02045, 1982.

Bacon, M. P. and Rosholt, J. N.: Accumulation rates of ^{230}Th, ^{231}Pa, and some transition metals on the Bermuda Rise, Geochim. Cosmochim. Ac., 46, 651–666, 1982.

Bacon, M. P., Huh, C. A. and Moore, R. M.: Vertical profiles of some natural radionuclides over the Alpha Ridge, Arctic Ocean, Earth Planet. Sc. Lett., 95, 15–22, https://doi.org/10.1016/0012-821X(89)90164-7, 1989.

Bradtmiller, L. I., Anderson, R. F., Fleisher, M. Q., and Burckle, L. H.: Opal burial in the equatorial Atlantic Ocean over the last 30 ka: Implications for glacial-interglacial changes in the ocean silicon cycle, Paleoceanography, 22, 1–15, https://doi.org/10.1029/2007PA001443, 2007.

Bradtmiller, L. I., McManus, J. F., and Robinson, L. F.: ^{231}Pa/^{230}Th evidence for a weakened but persistent Atlantic meridional overturning circulation during Heinrich Stadial 1, Nat. Commun., 5, 5817, https://doi.org/10.1038/ncomms6817, 2014.

Burckel, P., Waelbroeck, C., Luo, Y., Roche, D. M., Pichat, S., Jaccard, S. L., Gherardi, J., Govin, A., Lippold, J., and Thil, F.: Changes in the geometry and strength of the Atlantic meridional overturning circulation during the last glacial (20–50 ka), Clim. Past, 12, 2061–2075, https://doi.org/10.5194/cp-12-2061-2016, 2016.

Chase, Z. and Robert, F. A.: Comment on "On the importance of opal, carbonate, and lithogenic clays in scavenging and fractionating ^{230}Th, ^{231}Pa and ^{10}Be in the ocean" by S. Luo and T.-L. Ku, Earth Planet. Sc. Lett., 220, 201–211, https://doi.org/10.1016/S0012-821X(04)00027-5, 2004.

Chase, Z., Anderson, R. F., Fleisher, M. Q., and Kubik, P. W.: The influence of particle composition and particle flux on scavenging of Th, Pa and Be in the ocean, Earth Planet. Sc. Lett., 204, 215–229, https://doi.org/10.1016/S0012-821X(02)00984-6, 2002.

Cochran, J. K., Livingston, H. D., Hirschberg, D. J., and Surprenant, L. D.: Natural and anthropogenic radionuclide distributions in the northwest Atlantic Ocean, Earth Planet. Sci. Lett., 84, 135–152, https://doi.org/10.1016/0012-821X(87)90081-1, 1987.

Cochran, J. K., Hirschberg, D. J., Livingston, H. D., Buesseler, K. O., and Key, R. M.: Natural and anthropogenic radionuclide distributions in the Nansen Basin, Artic Ocean: Scavenging rates and circulation timescales, Deep-Sea Res. Pt. II, 42, 1495–1517, https://doi.org/10.1016/0967-0645(95)00051-8, 1995.

Colley, S., Thomson, J., and Newton, P. P.: Detailed ^{230}Th, ^{232}Th and ^{210}Pb fluxes recorded by the 1989/90 BOFS sediment trap time-series at 48° N, 20° W, Deep-Sea Res. Pt. I, 42, 833–848, https://doi.org/10.1016/0967-0637(95)00033-3, 1995.

Coppola, L., Roy-Barman, M., Mulsow, S., Povinec, P., and Jeandel, C.: Thorium isotopes as tracers of particles dynamics and deep water circulation in the Indian sector of the Southern Ocean (ANTARES IV), Mar. Chem., 100, 299–313, https://doi.org/10.1016/j.marchem.2005.10.019, 2006.

Danabasoglu, G., Bates, S. C., Briegleb, B. P., Jayne, S. R., Jochum, M., Large, W. G., Peacock, S., and Yeager, S. G.: The CCSM4 ocean component, J. Climate, 25, 1361–1389, https://doi.org/10.1175/JCLI-D-11-00091.1, 2012.

DeMaster, D. J.: The marine budgets of silica and ^{32}Si, PhD thesis, Yale Univ., New Haven, CT, USA, 1979.

Deng, F., Thomas, A. L., Rijkenberg, M. J. A., and Henderson, G. M.: Controls on seawater ^{231}Pa, ^{230}Th and ^{232}Th concentrations along the flow paths of deep waters in the Southwest Atlantic, Earth Planet. Sci. Lett., 390, 93–102, https://doi.org/10.1016/j.epsl.2013.12.038, 2014.

Doney, S. C., Lima, I., Feely, R. A., Glover, D. M., Lindsay, K., Mahowald, N., Moore, J. K., and Wanninkhof, R.: Mechanisms governing interannual variability in upper-ocean inorganic carbon system and air-sea CO_2 fluxes: Physical climate and atmospheric dust, Deep-Sea Res. Pt. II, 56, 640–655, https://doi.org/10.1016/j.dsr2.2008.12.006, 2009.

Dutay, J.-C., Lacan, F., Roy-Barman, M., and Bopp, L.: Influence of particle size and type on ^{231}Pa and ^{230}Th simulation with a global coupled biogeochemical-ocean general circulation model: A first approach, Geochem. Geophy. Geosy., 10, https://doi.org/10.1029/2008GC002291, 2009.

Edmonds, H. N., Moran, S. B., Hoff, J. A., Smith, J. N., and Edwards, R. L.: Protactinium-231 and Thorium-230 Abundances and High Scavenging Rates in the Western Arctic Ocean, Science, 280, 405–407, https://doi.org/10.1126/science.280.5362.405, 1998.

Edmonds, H. N., Moran, S. B., Cheng, H., and Edwards, R. L.: ^{230}Th and ^{231}Pa in the Arctic Ocean: Implications for particle fluxes and basin-scale Th/Pa fractionation, Earth Planet. Sc. Lett., 227, 155–167, https://doi.org/10.1016/j.epsl.2004.08.008, 2004.

Francois, R., Bacon, M. P., Altabet, M. A., and Labeyrie, L. D.: Glacial/interglacial changes in sediment rain rate in the SW Indian Sector of subantarctic Waters as recorded by ^{230}Th, ^{231}Pa, U, and δ^{15}N, Paleoceanography, 8, 611–629, https://doi.org/10.1029/93PA00784, 1993.

Frank, M.: Reconstruction of Late Quaternary environmental conditions applying the natural radionuclides ^{230}Th, ^{10}Be, ^{231}Pa and ^{238}U: A study of deep-sea sediments from the eastern sector of the Antarctic Circumpolar Current System, Alfred Wegener Institute for Polar and Marine Research, Bremerhaven, Germany, 1996.

Frank, M., Eisenhauer, A., Kubik, P. W., Dittrich-hannen, B. and Segl, M.: Beryllium 10, thorium 230, and protactinium 231 in Galapagos microplate sediments: Implications of hydrothermal activity and paleoproductivity changes during the last 100,000 years, Palaeogeography, 9, 559–578, 1994.

Geibert, W. and Usbeck, R.: Adsorption of thorium and protactinium onto different particle types: Experimental findings, Geochim. Cosmochim. Ac., 68, 1489–1501, https://doi.org/10.1016/j.gca.2003.10.011, 2004.

Gherardi, J., Labeyrie, L., Mcmanus, J., Francois, R., Skinner, L., and Cortijo, E.: Evidence from the Northeastern Atlantic basin for variability in the rate of the meridional overturning circulation through the last deglaciation, Earth Planet. Sc. Lett., 240, 710–723, https://doi.org/10.1016/j.epsl.2005.09.061, 2005.

Gherardi, J.-M., Labeyrie, L., Nave, S., Francois, R., McManus, J. F., and Cortijo, E.: Glacial-interglacial circulation changes inferred from 231 Pa/ 230 Th sedimentary record in the North Atlantic region, Paleoceanography, 24, https://doi.org/10.1029/2008PA001696, 2009.

Gu, S., Liu, Z., Zhang, J., Rempfer, J., Joos, J., Brady, E., and Oppo, D.: Coherent response of Antarctic Intermediate Water and Atlantic Meridional Overturning Circulation during the last deglaciation, Palaeogeography, https://doi.org/10.1002/2017PA003092, 2017.

Guo, L., Santschi, P. H., Baskaran, M., and Zindler, A.: Distribution of dissolved and particulate ^{230}Th and ^{232}Th in seawater from the Gulf of Mexico and off Cape Hatteras as measured by SIMS, Earth Planet. Sc. Lett., 133, 117–128, 1995.

Gutjahr, M., Frank, M., Stirling, C. H., Keigwin, L. D., and Halliday, A. N.: Tracing the Nd isotope evolution of North Atlantic Deep and Intermediate Waters in the western North Atlantic since the Last Glacial Maximum from Blake Ridge sediments, Earth Planet. Sc. Lett., 266, 61–77, https://doi.org/10.1016/j.epsl.2007.10.037, 2008.

Hall, I. R., Moran, S. B., Zahn, R., Knutz, P. C., Shen, C.-C., and Edwards, R. L.: Accelerated drawdown of meridional overturning in the late-glacial Atlantic triggered by transient pre-H event freshwater perturbation, Geophys. Res. Lett., 33, L16616, https://doi.org/10.1029/2006GL026239, 2006.

Hayes, C. T., Anderson, R. F., Fleisher, M. Q., Serno, S., Winckler, G., and Gersonde, R.: Quantifying lithogenic inputs to the North Pacific Ocean using the long-lived thorium isotopes, Earth Planet. Sc. Lett., 383, 16–25, https://doi.org/10.1016/j.epsl.2013.09.025, 2013.

Hayes, C. T., Anderson, R. F., Fleisher, M. Q., Huang, K. F., Robinson, L. F., Lu, Y., Cheng, H., Edwards, R. L. and Moran, S. B.: ^{230}Th and ^{231}Pa on GEOTRACES GA03, the U.S. GEOTRACES North Atlantic transect, and implications for modern and paleoceanographic chemical fluxes, Deep-Sea Res. Pt. II, 116, 29–41, https://doi.org/10.1016/j.dsr2.2014.07.007, 2015.

Henderson, G. M. and Anderson, R. F.: The U-series toolbox for paleoceanography, Rev. Mineral. Geochem., 52, 493–531, https://doi.org/10.2113/0520493, 2003.

Henderson, G. M., Heinze, C., Anderson, R. F., and Winguth, A. M. E.: Global distribution of the ^{230}Th flux to ocean sediments constrained by GCM modelling, Deep-Sea Res. Pt. I, 46, 1861–1893, https://doi.org/10.1016/S0967-0637(99)00030-8, 1999.

Hoffmann, S. S., McManus, J. F., Curry, W. B., and Brown-Leger, L. S.: Persistent export of ^{231}Pa from the deep central Arctic Ocean over the past 35,000 years, Nature, 497, 603–606, https://doi.org/10.1038/nature12145, 2013.

Hsieh, Y. Te, Henderson, G. M. and Thomas, A. L.: Combining seawater ^{232}Th and ^{230}Th concentrations to determine dust fluxes to the surface ocean, Earth Planet. Sc. Lett., 312, 280–290, https://doi.org/10.1016/j.epsl.2011.10.022, 2011.

Huh, C. A. and Beasley, T. M.: Profiles of dissolved and particulate thorium isotopes in the water column of coastal Southern California, Earth Planet. Sc. Lett., 85, 1–10, https://doi.org/10.1016/0012-821X(87)90016-1, 1987.

Hurrell, J. W., Holland, M. M., Gent, P. R., Ghan, S., Kay, J. E., Kushner, P. J., Lamarque, J. F., Large, W. G., Lawrence, D., Lindsay, K., Lipscomb, W. H., Long, M. C., Mahowald, N., Marsh, D. R., Neale, R. B., Rasch, P., Vavrus, S., Vertenstein, M., Bader, D., Collins, W. D., Hack, J. J., Kiehl, J., and Marshall, S.: The community earth system model: A framework for collaborative research, B. Am. Meteorol. Soc., 94, 1339–1360, https://doi.org/10.1175/BAMS-D-12-00121.1, 2013.

Jahn, A., Lindsay, K., Giraud, X., Gruber, N., Otto-Bliesner, B. L., Liu, Z., and Brady, E. C.: Carbon isotopes in the ocean model of the Community Earth System Model (CESM1), Geosci. Model Dev., 8, 2419–2434, https://doi.org/10.5194/gmd-8-2419-2015, 2015.

Jonkers, L., Zahn, R., Thomas, A., Henderson, G., Abouchami, W., François, R., Masque, P., Hall, I. R., and Bickert, T.: Deep circulation changes in the central South Atlantic during the past 145 kyrs reflected in a combined ^{231}Pa/^{230}Th, Neodymium isotope and benthic$_{\delta^{13}C}$ record, Earth Planet. Sc. Lett., 419, 14–21, https://doi.org/10.1016/j.epsl.2015.03.004, 2015.

Keigwin, L. D. and Boyle, E. A.: Did North Atlantic overturning halt 17,000 years ago?, Paleoceanography, 23, 1–5, https://doi.org/10.1029/2007PA001500, 2008.

Kriest, I.: Different parameterizations of marine snow in a 1D-model and their influence on representation of marine snow, nitrogen budget and sedimentation, Deep-Sea Res. Pt. I, 49, 2133–2162, https://doi.org/10.1016/S0967-0637(02)00127-9, 2002.

Ku, T. L.: Uranium series disequilibrium in deep sea sediments, Ph.D. Thesis, Columbia University, New York, 1966.

Ku, T. L., Bischoff, J. L., and Boersma, A.: Age studies of Mid-Atlantic Ridge sediments near 42°N and 20°N, Deep Sea Res. Oceanogr. Abstr., 19, 233–247, https://doi.org/10.1016/0011-7471(72)90033-2, 1972.

Kumar, N.: Trace metals and natural radionuclides as tracers of ocean productivity, PhD thesis, Columbia University, New York, 1994.

Kumar, N., Gwiazda, R., Anderson, R. F., and Froelich, P. N.: ^{231}Pa/^{230}Th ratios in sediments as a proxy for past changes in Southern Ocean productivity, Nature, 362, 45–48, https://doi.org/10.1038/362045a0, 1993.

Large, W. G. and Yeager, S. G.: The global climatology of an interannually varying air–sea flux data set, Clim. Dyn., 33, 341–364, https://doi.org/10.1007/s00382-008-0441-3, 2008.

Lippold, J., Grützner, J., Winter, D., Lahaye, Y., Mangini, A., and Christi, M.: Does sedimentary ^{231}Pa/^{230}Th from the Bermuda Rise monitor past Atlantic Meridional Overturning Circulation?, Geophys. Res. Lett., 36, L12601, https://doi.org/10.1029/2009GL038068, 2009.

Lippold, J., Gherardi, J. M., and Luo, Y.: Testing the ^{231}Pa / ^{230}Th paleocirculation proxy: A data versus 2D model comparison, Geophys. Res. Lett., 38, L20603, https://doi.org/10.1029/2011GL049282, 2011.

Lippold, J., Mulitza, S., Mollenhauer, G., Weyer, S., Heslop, D. and Christl, M.: Boundary scavenging at the East Atlantic margin does not negate use of ^{231}Pa/^{230}Th to trace Atlantic overturning, Earth Planet. Sc. Lett., 333–334, 317–331, https://doi.org/10.1016/j.epsl.2012.04.005, 2012a.

Lippold, J., Luo, Y., Francois, R., Allen, S. E., Gherardi, J., Pichat, S., Hickey, B., and Schulz, H.: Strength and geometry of the glacial Atlantic Meridional Overturning Circulation, Nat. Geosci., 5, 813–816, https://doi.org/10.1038/ngeo1608, 2012b.

Long, M. C., Lindsay, K., Peacock, S., Moore, J. K., and Doney, S. C.: Twentieth-century oceanic carbon uptake and storage in CESM1(BGC), J. Climate, 26, 6775–6800, https://doi.org/10.1175/JCLI-D-12-00184.s1, 2013.

Luo, S. and Ku, T. L.: Oceanic ^{231}Pa/^{230}Th ratio influenced by particle composition and remineralization, Earth Planet. Sc. Lett., 167, 183–195, https://doi.org/10.1016/S0012-821X(99)00035-7, 1999.

Luo, S. D., Ku, T. L., Kusakabe, M., Bishop, J. K. B., and Yang, Y. L.: Tracing particle cycling in the upper ocean with ^{230}Th and ^{228}Th: An investigation in the equatorial Pacific along 140°W, Deep-Sea Res. Pt. II, 42, 805–829, https://doi.org/10.1016/0967-0645(95)00019-M, 1995.

Luo, Y., Francois, R., and Allen, S.: Sediment ^{231}Pa/^{230}Th as a recorder of the rate of the Atlantic meridional overturning circulation: insights from a 2-D model, Ocean Sci., 6, 381–400, https://doi.org/10.5194/os-6-381-2010, 2010.

Mangini, A. and Diester-Hass, L.: Excess Th-230 in sediments off NW Africa traces upwelling during the past 130,000 years, in: Coastal upwelling: Its sedimentary records, edited by: Suess, E. and Thiede, J., Plenum Press, Springer US, New York, 455–470, 1983.

Mangini, A. and Key, R. M.: A ^{230}Th profile in the Atlantic Ocean, Earth Planet. Sc. Lett., 62, 377–384, https://doi.org/10.1016/0012-821X(83)90008-0, 1983.

Mangini, A. and Sonntag, C.: ^{231}Pa dating of deep-sea cores via 227Th counting, Earth Planet. Sc. Lett., 37, 251–256, https://doi.org/10.1016/0012-821X(77)90170-4, 1977.

Mangini, A. and Kühnel, U.: Depositional history in the Clarion-Clipperton zone during the last 250,000 years: ^{230}Th and ^{231}Pa methods, Geol. Jahrb., 87, 105–121, 1987.

Marchal, O., François, R., Stocker, T. F., and Joos, F.: Ocean thermohaline circulation and sedimentary ^{231}Pa/^{230}Th ratio, Paleoceanography, 15, 625–641, https://doi.org/10.1029/2000PA000496, 2000.

McManus, J., Francois, R., and Gherardi, J.: Collapse and rapid resumption of Atlantic meridional circulation linked to deglacial climate changes, Nature, 428, 834–837, 2004.

Moore, J. K. and Braucher, O.: Sedimentary and mineral dust sources of dissolved iron to the world ocean, Biogeosciences, 5, 631–656, https://doi.org/10.5194/bg-5-631-2008, 2008.

Moore, J. K., Doney, S. C., Glover, D. M. and Fung, I. Y.: Iron cycling and nutrient-limitation patterns in surface waters of the World Ocean, Deep-Sea Res. Pt. II, 49, 463–507, https://doi.org/10.1016/S0967-0645(01)00109-6, 2002.

Moore, J. K., Doney, S. C., and Lindsay, K.: Upper ocean ecosystem dynamics and iron cycling in a global three-dimensional model, Global Biogeochem. Cycles, 18(4), https://doi.org/10.1029/2004GB002220, 2004.

Moore, J. K., Lindsay, K., Doney, S. C., Long, M. C., and Misumi, K.: Marine Ecosystem Dynamics and Biogeochemical Cycling in the Community Earth System Model [CESM1(BGC)]: Comparison of the 1990s with the 2090s under the RCP4.5 and RCP8.5 Scenarios, J. Climate, 26, 9291–9312, https://doi.org/10.1175/JCLI-D-12-00566.1, 2013.

Moore, R. M. and Hunter, K. A.: Thorium adsorption in the ocean: reversibility and distribution amongst particle sizes, Geochim. Cosmochim. Ac., 49, 2253–2257, https://doi.org/10.1016/0016-7037(85)90225-X, 1985.

Moore, W. S.: The thorium isotope content of ocean water, Earth Planet. Sc. Lett., 53, 419–426, https://doi.org/10.1016/0012-821X(81)90046-7, 1981.

Moran, S. B., Hoff, J. A., Buesseler, K. O., and Edwards, R. L.: High precision ^{230}Th and ^{232}Th in the Norwegian Sea and Denmark by thermal ionization mass spectrometry, , 22, 2589–2592, 1995.

Moran, S. B., Charette, M. A., Hoff, J. A., Edwards, R. L., and Landing, W. M.: Distribution of ^{230}Th in the Labrador Sea and its relation to ventilation, Earth Planet. Sc. Lett., 150, 151–160, https://doi.org/10.1016/S0012-821X(97)00081-2, 1997.

Moran, S. B., Shen, C.-C., Weinstein, S. E., Hettinger, L. H., Hoff, J. H., E dmonds, H. N., and Edwards, R. L.: Constraints on deep water age and particle flux in the Equatorial and South Atlantic Ocean based on seawater ^{231}Pa and ^{230}Th data, Geophys. Res. Lett., 28, 3437–3440, 2001.

Moran, S. B., Shen, C. C., Edmonds, H. N., Weinstein, S. E., Smith, J. N., and Edwards, R. L.: Dissolved and particulate ^{231}Pa and ^{230}Th in the Atlantic Ocean: Constraints on intermediate/deep water age, boundary scavenging, and ^{231}Pa/^{230}Th fractionation, Earth Planet. Sc. Lett., 203, 999–1014, https://doi.org/10.1016/S0012-821X(02)00928-7, 2002.

Müller, P. J. and Mangini, A.: Organic carbon decomposition rates in sediments of the pacific manganese nodule belt dated by ^{230}Th and ^{231}Pa, Earth Planet. Sc. Lett., 51, 94–114, https://doi.org/10.1016/0012-821X(80)90259-9, 1980.

Negre, C., Zahn, R., Thomas, A. L., Masqué, P., Henderson, G. M., Martínez-Méndez, G., Hall, I. R., and Mas, J. L.: Reversed flow of Atlantic deep water during the Last Glacial Maximum., Nature, 468, 84–88, https://doi.org/10.1038/nature09508, 2010.

Nozaki, Y. and Horibe, Y.: Alpha-emitting thorium isotopes in northwest Pacific deep waters, Earth Planet. Sc. Lett., 65, 39–50, https://doi.org/10.1016/0012-821X(83)90188-7, 1983.

Nozaki, Y. and Nakanishi, T.: ^{231}Pa and ^{230}Th profiles in the open ocean water column, Deep-Sea Res. Pt. A-Oceanogr. Res. Pap., 32, 1209–1220, https://doi.org/10.1016/0198-0149(85)90004-4, 1985.

Nozaki, Y. and Yamada, M.: Thorium and protactinium isotope distributions in waters of the Japan Sea, Deep-Sea Res. Pt. A-Oceanogr. Res. Pap., 34, 1417–1430, 1987.

Nozaki, Y. and Yang, H. S.: Th and Pa isotopes in the waters of the western margin of the pacific near Japan: Evidence for release of228Ra and227Ac from slope sediments, J. Oceanogr. Soc. Japan, 43, 217–227, https://doi.org/10.1007/BF02109817, 1987.

Nozaki, Y., Horibe, Y., and Tsubota, H.: The water column distribution of thorium isotopes in the western North Pacific, Earth Planet. Sc. Lett., 54, 203–216, 1981.

Nozaki, Y., Yang, H.-S., and Yamada, M.: Scavenging of thorium in the ocean, J. Geophys. Res., 92, 772, https://doi.org/10.1029/JC092iC01p00772, 1987.

Okubo, A., Obata, H., Nozaki, Y., Yamamoto, Y., and Minami, H.: ^{230}Th in the Andaman Sea: Rapid deep-sea renewal, Geophys. Res. Lett., 31, 1–5, https://doi.org/10.1029/2004GL020226, 2004.

Okubo, A., Obata, H., Luo, S., Gamo, T., Yamamoto, Y., Minami, H., and Yamada, M.: Particle flux in the twilight zone of the eastern Indian Ocean: A constraint from ^{234}U-^{230}Th and ^{228}Ra-^{228}Th disequilibria, Deep-Sea Res. Pt. I, 54, 1758–1772, https://doi.org/10.1016/j.dsr.2007.06.009, 2007a.

Okubo, A., Obata, H., Gamo, T., Minami, H. and Yamada, M.: Scavenging of ^{230}Th in the Sulu Sea, Deep-Sea Res. Pt. II, 54, 50–59, https://doi.org/10.1016/j.dsr2.2006.02.016, 2007b.

Okubo, A., Obata, H., Gamo, T., and Yamada, M.: ^{230}Th and 232Th distributions in mid-latitudes of the North Pacific Ocean: Effect of bottom scavenging, Earth Planet. Sc. Lett., 339–340, 139–150, https://doi.org/10.1016/j.epsl.2012.05.012, 2012.

Rempfer, J., Stocker, T. F., Joos, F., Lippold, J., and Jaccard, S. L.: New insights into cycling of ^{231}Pa and ^{230}Th in the Atlantic Ocean, Earth Planet. Sc. Lett., 468, 27–37, https://doi.org/10.1016/j.epsl.2017.03.027, 2017.

Roberts, N. L., McManus, J. F., Piotrowski, A. M., and McCave, I. N.: Advection and scavenging controls of Pa/Th in the northern NE Atlantic, Paleoceanography, 29, 668–679, https://doi.org/10.1002/2014PA002633, 2014.

Robinson, L. F., Belshaw, N. S., and Henderson, G. M.: U and Th concentrations and isotope ratios in modern carbonates and waters from the Bahamas, Geochim. Cosmochim. Ac., 68, 1777–1789, https://doi.org/10.1016/j.gca.2003.10.005, 2004.

Roy-Barman, M., Chen, J. H., and Wasserburg, G. J.: ^{230}Th-232Th systematics in the central Pacific Ocean: The sources and the fates of thorium, Earth Planet. Sc. Lett., 139, 351–363, https://doi.org/10.1016/0012-821X(96)00017-9, 1996.

Rutgers van der Loeff, M. M. and Berger, G. W.: Scavenging of ^{230}Th and ^{231}Pa near the antarctic polar front in the South Atlantic, Deep-Sea Res. Pt. I, 40, 339–357, https://doi.org/10.1016/0967-0637(93)90007-P, 1993.

Sarmiento, J. L. and Gruber, N.: Ocean Biogeochemical Dynamics, Princeton University Press, 2006.

Schmittner, A.: Decline of the marine ecosystem caused by a reduction in the Atlantic overturning circulation, Nature, 434, 628–633, https://doi.org/10.1038/nature03476, 2005.

Schmitz, W., Mangini, A., Stoffers, P., Glasby, G. P., and Pluger, W. L.: Sediment accumulation rates in the southwestern Pacific Basin and Aitutaki Passage, Mar. Geol., 73, 181–190, 1986.

Scholten, J. C., Rutgers van der Loeff, M. M., and Michel, A.: Distribution of ^{230}Th and ^{231}Pa in the water column in relation to the ventilation of the deep Arctic basins, Deep-Sea Res. Pt. II, 42, 1519–1531, https://doi.org/10.1016/0967-0645(95)00052-6, 1995.

Scholten, J. C., Fietzke, J., Mangini, A., Stoffers, P., Rixen, T., Gaye-Haake, B., Blanz, T., Ramaswamy, V., Sirocko, F., Schulz, H., and Ittekkot, V.: Radionuclide fluxes in the Arabian Sea: The role of particle composition, Earth Planet. Sc. Lett., 230, 319–337, https://doi.org/10.1016/j.epsl.2004.11.003, 2005.

Scholten, J. C., Fietzke, J., Mangini, A., Garbe-Schönberg, C. D., Eisenhauer, A., Schneider, R., and Stoffers, P.: Advection and scavenging: Effects on ^{230}Th and ^{231}Pa distribution off Southwest Africa, Earth Planet. Sc. Lett., 271, 159–169, https://doi.org/10.1016/j.epsl.2008.03.060, 2008.

Shimmield, G. B. and Price, N. B.: The scavenging of U, ^{230}Th and ^{231}Pa during pulsed hydrothermal activity at 20° S, East Pacific Rise, Geochim. Cosmochim. Ac., 52, 669–677, https://doi.org/10.1016/0016-7037(88)90329-8, 1988.

Shimmield, G. B., Murray, J. W., Thomson, J., Bacon, M. P., Anderson, R. F., and Price, N. B.: The distribution and behaviour of ^{230}Th and ^{231}Pa at an ocean margin, Baja California, Mexico, Geochim. Cosmochim. Ac., 50, 2499–2507, https://doi.org/10.1016/0016-7037(86)90032-3, 1986.

Siddall, M., Henderson, G. M., Edwards, N. R., Frank, M., Müller, S. A., Stocker, T. F., and Joos, F.: ^{231}Pa/^{230}Th fractionation by ocean transport, biogenic particle flux and particle type, Earth Planet. Sc. Lett., 237, 135–155, https://doi.org/10.1016/j.epsl.2005.05.031, 2005.

Siddall, M., Stocker, T. F., Henderson, G. M., Joos, F., Frank, M., Edwards, N. R., Ritz, S. P., and Müller, S. A.: Modeling the relationship between ^{231}Pa/^{230}Th distribution in North Atlantic sediment and Atlantic meridional overturning circulation, Paleoceanography, 22, PA2214, https://doi.org/10.1029/2006PA001358, 2007.

Thomas, A. L., Henderson, G. M., and Robinson, L. F.: Interpretation of the ^{231}Pa/^{230}Th paleocirculation proxy: New water-column measurements from the southwest Indian Ocean, Earth Planet. Sc. Lett., 241, 493–504, https://doi.org/10.1016/j.epsl.2005.11.031, 2006.

Trimble, S. M., Baskaran, M., and Porcelli, D.: Scavenging of thorium isotopes in the Canada Basin of the Arctic Ocean, Earth Planet. Sc. Lett., 222, 915–932, https://doi.org/10.1016/j.epsl.2004.03.027, 2004.

Venchiarutti, C., van der Loeff, M. R., and Stimac, I.: Scavenging of ^{231}Pa and thorium isotopes based on dissolved and size-fractionated particulate distributions at Drake Passage (ANTXXIV-3), Deep-Sea Res. Pt. II, 58, 2767–2784, https://doi.org/10.1016/j.dsr2.2010.10.040, 2011.

Vogler, S., Scholten, J., Rutgers van der Loeff, M. M., and Mangini, A.: ^{230}Th in the eastern North Atlantic: the importance of water mass ventilation in the balance of ^{230}Th, Earth Planet. Sc. Lett., 156, 61–74, https://doi.org/10.1016/S0012-821X(98)00011-9, 1998.

Walter, H. J., Rutgers van der Loeff, M. M., and Hoeltzen, H.: Enhanced scavenging of ^{231}Pa relative to ^{230}Th in the South Atlantic south of the Polar Front: Implications for the use of the ^{231}Pa/^{230}Th ratio as a paleoproductivity proxy, Earth Planet. Sc. Lett., 149, 85–100, https://doi.org/10.1016/S0012-821X(97)00068-X, 1997.

Yang, H. S., Nozaki, Y., Sakai, H., and Masuda, A.: The distribution of ^{230}Th and ^{231}Pa in the deep-sea surface sediments of the Pacific Ocean, Geochim. Cosmochim. Ac., 50, 81–89, https://doi.org/10.1016/0016-7037(86)90050-5, 1986.

Yong-Liang Yang, Elderfield, H., Pedersen, T. F., and Ivanovich, M.: Geochemical record of the Panama Basin during the Last Glacial Maximum carbon event shows that the glacial ocean was not suboxic, Geology, 23, 1115–1118, https://doi.org/10.1130/0091-7613(1995)023<1115:GROTPB>2.3.CO;2, 1995.

Yong Lao, Anderson, R. F., Broecker, W. S., Trumbore, S. E., Hofmann, H. J., and Wolfli, W.: Transport and burial rates of ^{10}Be and ^{231}Pa in the Pacific Ocean during the Holocene period, Earth Planet. Sc. Lett., 113, 173–189, https://doi.org/10.1016/0012-821X(92)90218-K, 1992.

Yu, E.-F.: Variations in the Particulate Flux of ^{230}Th and ^{231}Pa and Paleoceanographic Applications of the ^{231}Pa/^{230}Th Ratio, PhD thesis, Woods Hole Oceanographic Institution, Massachusetts Institute of Technology, 1994.

Yu, E.-F., Francois, R., and Bacon, M. P.: Similar rates of modern and last-glacial ocean thermohaline circulation inferred from radiochemical data, Nature, 379, 689–694, https://doi.org/10.1038/379689a0, 1996.